ARMY RESEARCH LABORATORY

Lightweight, Durable Army Antennas Using Carbon Nanotube Technology (Final Report)

by Steven D. Keller and Amir I. Zaghloul

ARL-TR-6323 **January 2013**

NOTICES

Disclaimers

The findings in this report are not to be construed as an official Department of the Army position unless so designated by other authorized documents.

Citation of manufacturer's or trade names does not constitute an official endorsement or approval of the use thereof.

Destroy this report when it is no longer needed. Do not return it to the originator.

Army Research Laboratory
Adelphi, MD 20783-1197

ARL-TR-6323 **January 2013**

Lightweight, Durable Army Antennas Using Carbon Nanotube Technology (Final Report)

Steven D. Keller and Amir I. Zaghloul
Sensors and Electron Devices Directorate, ARL

REPORT DOCUMENTATION PAGE	Form Approved OMB No. 0704-0188

1. REPORT DATE *(DD-MM-YYYY)*	2. REPORT TYPE	3. DATES COVERED (From - To)
January 2013	DRI	1 October 2011 to 30 September 2012

4. TITLE AND SUBTITLE
Lightweight, Durable Army Antennas Using Carbon Nanotube Technology (Final Report)

5a. CONTRACT NUMBER

5b. GRANT NUMBER

5c. PROGRAM ELEMENT NUMBER

6. AUTHOR(S)
Steven D. Keller, Amir I. Zaghloul

5d. PROJECT NUMBER
FY11-SED-028

5e. TASK NUMBER

5f. WORK UNIT NUMBER

7. PERFORMING ORGANIZATION NAME(S) AND ADDRESS(ES)
U.S. Army Research Laboratory
ATTN: RDRL-SER-M
Adelphi, MD 20783-1197

8. PERFORMING ORGANIZATION REPORT NUMBER
ARL-TR-6323

9. SPONSORING/MONITORING AGENCY NAME(S) AND ADDRESS(ES)

10. SPONSOR/MONITOR'S ACRONYM(S)

11. SPONSOR/MONITOR'S REPORT NUMBER(S)

12. DISTRIBUTION/AVAILABILITY STATEMENT
Approved for public release; distribution unlimited.

13. SUPPLEMENTARY NOTES

14. ABSTRACT
The application of carbon nanotube (CNT) materials to produce lightweight, flexible, and durable alternatives to existing and future Army antenna designs is explored through fabrication and measurement of a variety of CNT thread and sheet antenna designs. A variety of CNT thread/rope dipole and loop antennas are fabricated, measured, and compared with a standard copper dipole antenna. An aperture-coupled patch antenna composed of CNT sheet material, is fabricated, measured, and compared with a standard copper patch antenna. Finally, a meshed patch antenna composed of interwoven CNT threads is developed and simulated as a concept for a multifunctional communications antenna and reactive gas sensor.

15. SUBJECT TERMS
Carbon nanotube, antenna, array, dipole, Method of Moments, Director's Research Initiative (DRI)

16. SECURITY CLASSIFICATION OF:			17. LIMITATION OF ABSTRACT	18. NUMBER OF PAGES	19a. NAME OF RESPONSIBLE PERSON
a. REPORT	b. ABSTRACT	c. THIS PAGE			Steven D. Keller
Unclassified	Unclassified	Unclassified	UU	48	19b. TELEPHONE NUMBER (*Include area code*) (301)394-0576

Standard Form 298 (Rev. 8/98)
Prescribed by ANSI Std. Z39.18

Contents

List of Figures

Acknowledgments

We thank Dr. Vesselin Shanov, Dr. Mark Schulz and Dr. David Mast of the NanoWorld Laboratory at the University of Cincinnati for fabricating and measuring carbon nanotube thread samples and providing carbon nanotube sheet materials for this research under U.S. Army Research Laboratory (ARL) Cooperative Agreement # W911NF-12-2-0031. We also thank the Director's Research Initiative (DRI) committee for providing the opportunity and resources to conduct the research for this program in FY11 and FY12.

1. Objective

Many functional challenges exist when wireless systems are integrated onto an Army vehicle or a Soldier's pack, uniform, or handheld equipment. Typical antennas for these systems are often visually compromising and cumbersome to the Soldier. Antennas fabricated from standard conductive materials such as copper fail to stand up to significant "wear-and-tear" due to lack of durability and are thus limited in their placement to areas on the platform (uniform, pack, etc.) that see minimal flexing and bending. Thus, size/weight reduction and enhanced conformability and durability of Army antennas perennially exist as overarching Army antenna research objectives.

Carbon nanotubes (CNTs) have recently emerged as an attractive material, both physically and electrically, due to its extremely light weight, durability, and conductive properties. While the application of an individual single-wall nanotube (SWNT) as an antenna has been analytically shown to yield very low radiation efficiency at microwave frequencies (*1*, *2*), it has recently been shown through analysis (*3*, *4*) and measurement (*5*) that the dominant kinetic inductance and resistance of a CNT can be significantly reduced by fabricating a large number of CNTs into a bundle structure. It has also been predicted through simulations that dipole antennas constructed from CNT bundle structures may exhibit radiation efficiency orders of magnitude higher than that of individual CNTs (*6*) and that this radiation efficiency increases as the nanotube density with the bundle is increased (*7*). Emerging fabrication techniques have made realizable the synthesis of large-scale CNT bundle structures such as threads, ribbons, and sheets (*8*). By using these CNT threads to produce wireframe antennas and CNT sheets/ribbons to produce planar and waveguide antennas, it may be possible to fabricate antennas with significantly reduced weight and enhanced flexibility, durability, and power handling capabilities when compared with antenna structures fabricated out of traditional bulk conductive materials (*9*). The objective of this research is to explore the latest advances in CNT materials and how they may be applied to Army antenna designs to produce lightweight, flexible, and conformal alternatives to existing and future Army antennas.

2. DRI Year 1 Review

In year 1 of this Director's Research Initiative (DRI), the application of CNT thread/rope to radio frequency (RF) antenna designs was explored through conductivity and dipole antenna simulation and the measurement and analysis of the physical and electrical characteristics of CNT thread/rope samples. The simulation results indicated that CNT thread/rope conductivity improves with increased diameter (ply) and that the application of these materials as a half

wavelength dipole antenna yields manageable losses of less than 1 to 5 dB at RF frequencies above 10 GHz.

According to the measured results obtained from the CNT thread/rope samples fabricated by the University of Cincinnati, the most significant physical benefit to be gained by employing CNT thread versus copper wire was a reduction in conductor weight. Contrary to what was expected from intuition and simulation results, the tensile strength and conductivity of the multi-ply CNT rope samples actually decreased with larger ply rope (multi-thread braided structures) and was less than that of the single ply CNT thread samples. Thus, single-ply CNT thread should be focused on for future research. Applying a post-fabrication treatment of dimethyl sulfoxide (DMSO) to the CNT threads was found to be an important step in enhancing the physical and electrical characteristics of the material. The tensile strength exhibited by the DMSO-treated single-ply CNT thread was ~2.5 times greater than that exhibited by the untreated sample and was approximately the same as that of copper wire. With thermal annealing applied as an additional post-process treatment, it is expected that the conductivity should improve to at least 1e6 S/m (still lower than copper but more competitive) and the tensile strength should improve to ~1 GPa (much higher than copper). Improvement of the tensile strength to far beyond that of copper will be an important step in justifying the use of CNT thread materials as a substitute for a traditional conductive material. As bulk CNT thread fabrication capabilities are refined and costs are lowered (typical cost in 2011 is ~$400 per gram multiwall nanotubes [MWNTs] forest or 8 cents per meter of CNT thread), these materials should become an attractive alternative conductive material for weight-restricted and uniform-integrated Army antenna applications.

Additionally, the first steps were taken towards establishing patterned vertically aligned multiwall CNT (MWNT) array fabrication capabilities at the U.S. Army Research Laboratory (ARL). A variety of patterned CNT arrays were successfully fabricated on silicon (Si) wafers, with pattern sizes ranging from 5 μm to 2 mm. Attempts at fabricating MWNT arrays using an iron thin-film catalyst were ultimately unsuccessful since the nanotubes did not adhere well to the substrate. While future research will be needed to produce sustainable vertically aligned MWNT growth capabilities at ARL, the patterned CNT array fabrication capabilities developed under this program will be applicable to future Army research of planar CNT antenna arrays. Due to the realignment of RDRL-SER-L branch focus on graphene fabrication versus CNT array fabrication, this part of the DRI research was not continued in year 2.

Year 2 of this DRI focused on the fabrication and measurement of a variety of CNT thread and sheet antenna designs, as well as on the development of an innovative multifunctional CNT patch antenna/gas sensor. A variety of CNT thread/rope dipole and loop antennas were fabricated, measured, and compared with a standard copper dipole antenna. A more complex CNT antenna structure, an aperture-coupled patch antenna comprised of CNT sheet material, was also fabricated and compared with a standard copper patch antenna. Finally, a variation on this design using interwoven CNT threads to form a meshed thread patch antenna was developed and simulated as a concept for a multifunctional communications antenna and reactive gas sensor.

3. Results

3.1 Carbon Nanotube Thread Antennas

As a continuation of the research started in DRI year 1 on the application of CNT thread materials to RF antenna designs, a variety of CNT dipole and loop antennas were fabricated and measured using the CNT thread that was developed and characterized in collaboration with the University of Cincinnati. In order to formalize this collaboration and enable better research flexibility, a Cooperative Agreement (W911NF-12-2-0031) was established with the University of Cincinnati through the Army Research Office in May 2012.

A conceptual diagram of a half wavelength (λ/2) CNT thread dipole antenna is shown in figure 1 (*10*). The dipole thread is composed of many thousands of individual double-wall CNTs with typical diameter of 10–12 nm held together by van der Waals forces and spun to form a strong, thread-like structure with a typical overall diameter of ~20–25 µm. These are connected to the output of a balun to match the balanced dipole load to an unbalanced coaxial feed connector and provide a 180° phase difference between the signal excitation in each leg of the dipole.

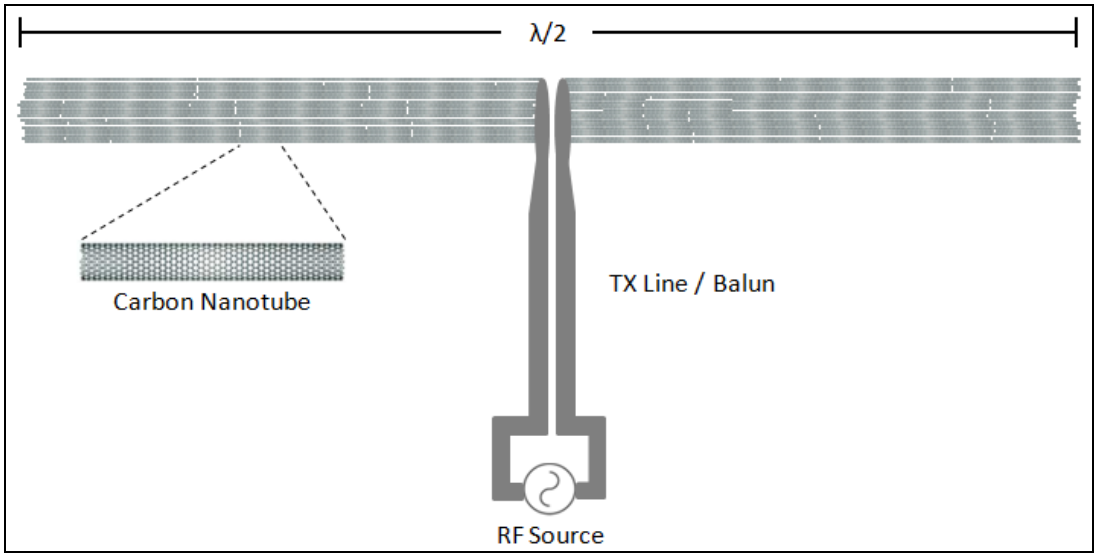

Figure 1. CNT thread dipole antenna concept.

As originally described in the DRI year 1 final report, a variety of CNT thread and rope samples were fabricated by the University of Cincinnati to apply to the construction of CNT thread/rope dipole antenna prototypes. The fabrication technique employed to produce this thread is detailed in figure 2.

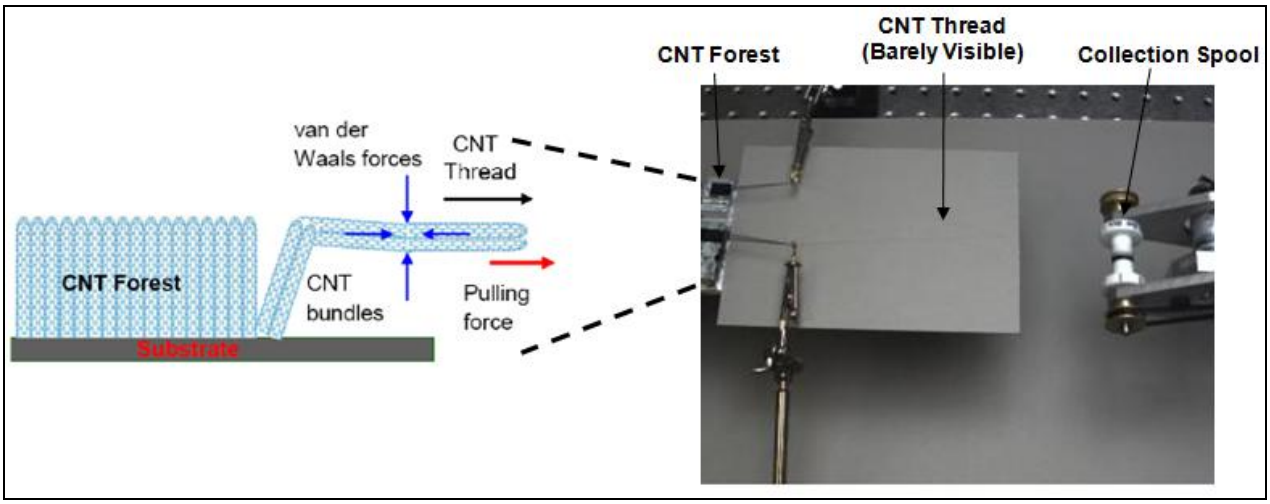

Figure 2. CNT thread fabrication technique at University of Cincinnati NanoWorld Laboratory (adapted from reference 8).

A dense array of vertically aligned MWNTs (typically 10–12 nm diameter double-wall CNTs) are grown using a chemical vapor deposition (CVD) process on a 4-in Si wafer with a density of approximately 0.03 gm/cm^3 and an average tube length of 500 µm. By means of a proprietary method, the MWNTs are collected and spun into a thread-like structure, with the individual nanotube bundles held together by van der Waals forces. The final 1-ply thread is typically 20–25 µm in diameter. By performing the same spinning process with multiple spools of 1-ply thread, a variety of larger ply CNT rope was fabricated, including a 3-ply CNT rope and a 3x3-ply CNT rope (three 3-ply CNT ropes spun together).

An additional post-processing technique of applying DMSO to the CNT thread/rope samples was explored to enhance the thread conductivity and tensile strength. In this process, the capillary forces caused by the evaporation of the applied DMSO solvent draw the neighboring CNTs within the threads closer together and yield a denser thread structure. This process both reduces the CNT thread/rope diameter and enhances the ability to work with and handle the samples. These standard and DMSO-densified samples were fabricated in DRI year 1 under ARL contract #W911QX11P0132 with contract period from April 2011–January 2012 and their physical and electrical properties were measured and analyzed. The samples were provided to ARL for the construction and measurement of CNT thread dipole antenna and meshed CNT thread patch antenna prototypes. Images of the CNT thread/rope samples were captured using an environmental scanning electron microscope (ESEM), as shown in figures 3 through 5 (*10*).

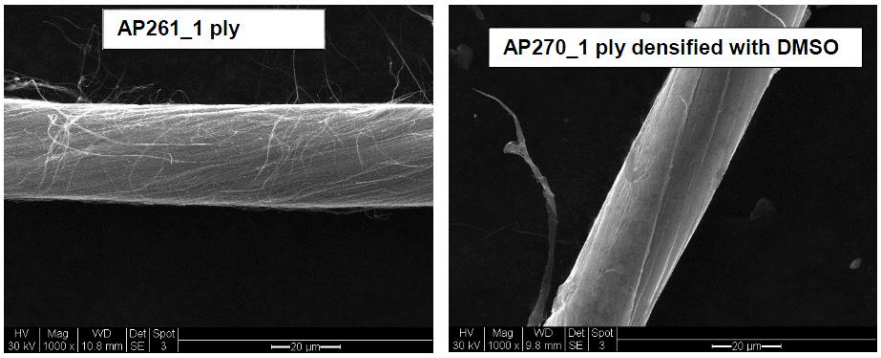

Figure 3. ESEM images of standard and DMSO densified 1-ply CNT thread.

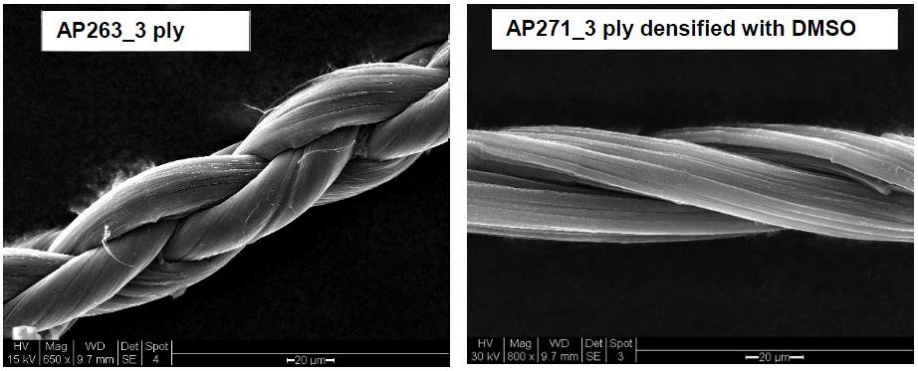

Figure 4. ESEM images of standard and DMSO densified 3-ply CNT rope.

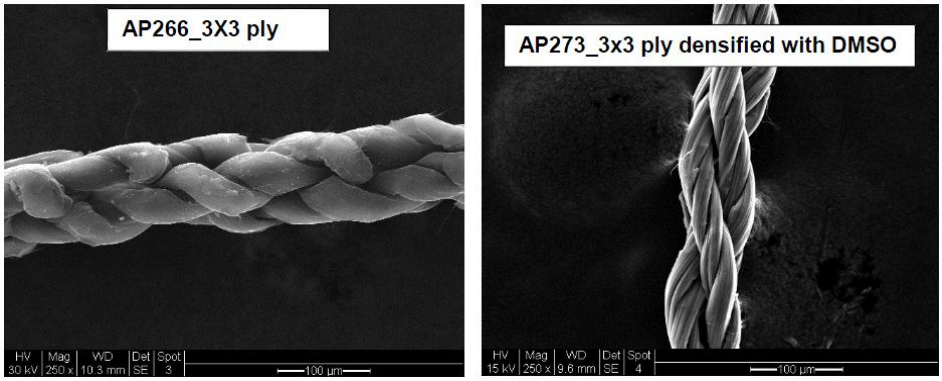

Figure 5. ESEM images of standard and DMSO densified 3x3-ply CNT rope.

3.1.1 CNT Thread Dipole Antenna

A variety of CNT thread/rope dipole antennas were constructed on low-loss foam board using the CNT thread and rope provided by the University of Cincinnati, with an accompanying balun (1:1 and 4:1 versions) attached to provide a 180° phase shift between the two dipole legs. To achieve an electrical connection between the CNT threads and an SMA connector, a short length of copper wire was inserted between the thread and connector center conductor and silver paste was applied and cured. For comparison, a baseline dipole antenna composed of 40-gauge copper wire was also constructed. Select images of these prototypes are shown in figure 6.

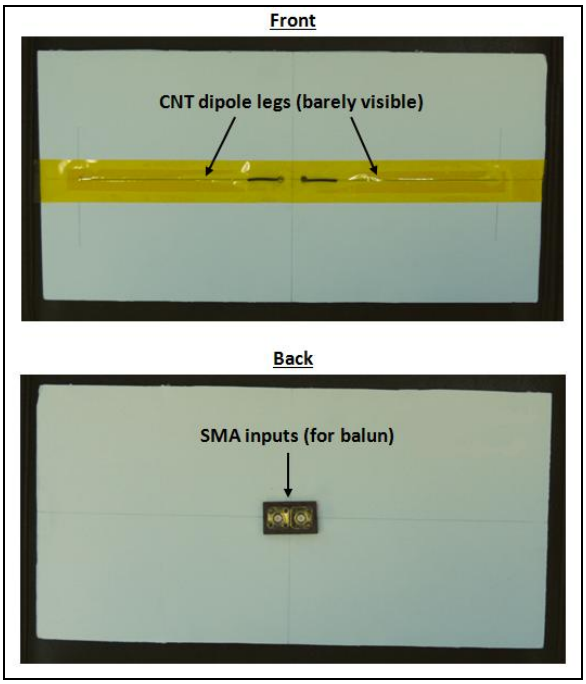

Figure 6. CNT thread/rope dipole antenna prototype.

In early measurements of these dipole antennas, concerns arose regarding the balun designs and copper wire connection methods and whether they were contributing significantly to the measured performance of the antennas. The measured reflection coefficient data for each of the antenna prototypes is shown in figures 7 and 8.

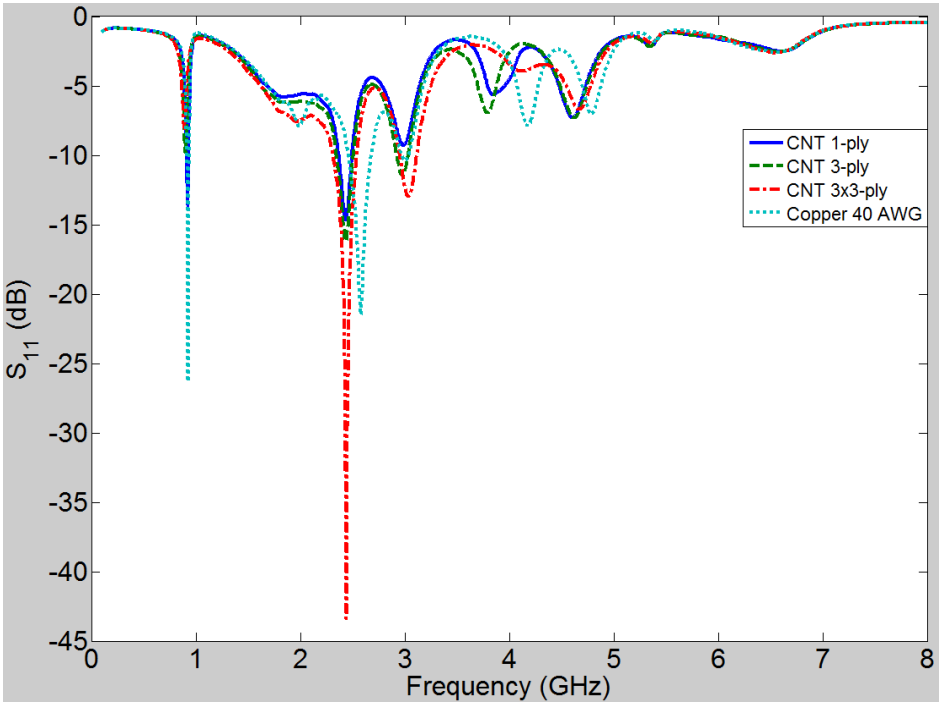

Figure 7. Measured reflection coefficient for 2-in CNT thread/rope and copper dipole antennas.

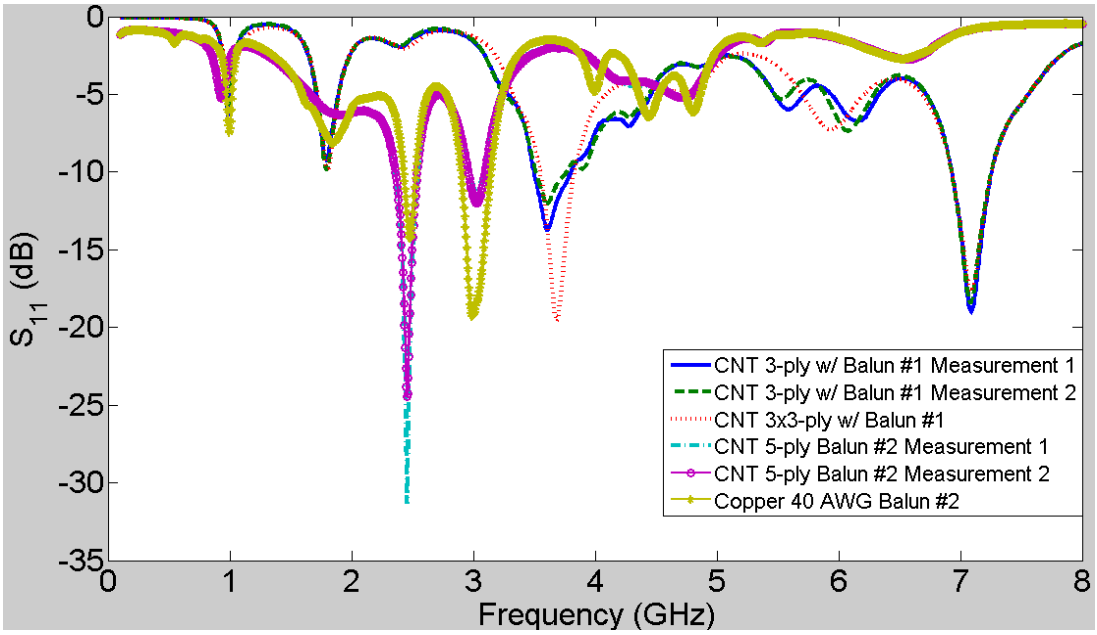

Figure 8. Measured reflection coefficient for 10-in CNT thread/rope and copper dipole antennas.

Two different baluns (a 1:1 and a 4:1 balun) were used for these measurements. The 1:1 balun (Balun #2) was used for all 2.5-in dipole prototypes and for the 5-ply and copper 11-in-long dipole antennas. The 4:1 balun (Balun #1) was used for the 3-ply and 3x3-ply 11-in-long CNT dipole antennas. From the measured reflection coefficient plots, it can clearly be seen that a resonance occurs where it is expected to for the 2.5-in dipole (f_0 = 2.4 GHz), but does not for the 11-in dipole (expected f_0 = 536 MHz). A prominent resonance is seen at both ~1 and 2.4 GHz for all antennas with the 1:1 balun attached, including the 2.5- and 11-in-long antennas, which indicates that they are not operating as λ/2 dipole antennas. Indeed, the overall reflection coefficient responses from 100 MHz to 8 GHz for each of the 2.5- and 11-in antennas that used Balun #2 are nearly identical. Functional λ/2 dipole antennas of considerably different lengths should have significantly different reflection coefficient measurements, with a strong resonance at the frequency corresponding to its half wavelength in free space.

For this reason, the decision was made to remove the balun from these designs and make measurements on just one leg of each of dipole antenna, effectively turning each prototype into an unbalanced λ/4 stub antenna (monopole without a ground plane). The measured reflection coefficient data for the CNT thread and copper 1.25- and 5-in stub antennas is shown in figures 9 and 10.

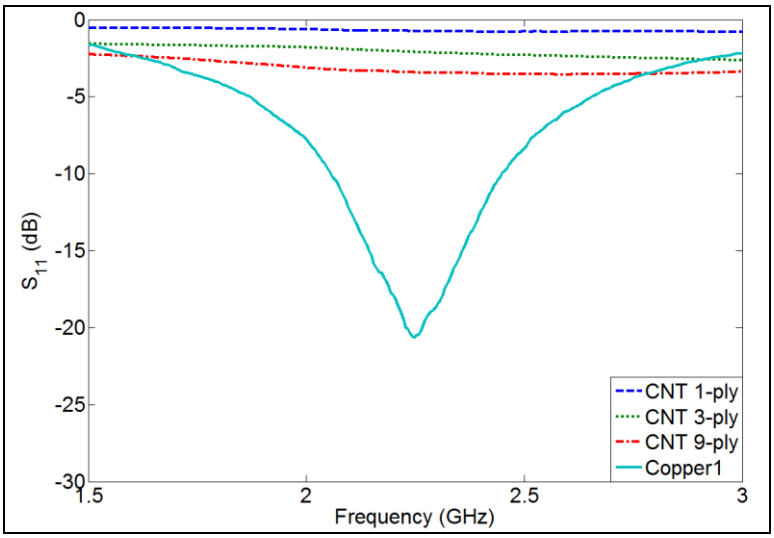

Figure 9. Measured reflection coefficient for 1.25-in CNT thread/rope and copper stub antennas.

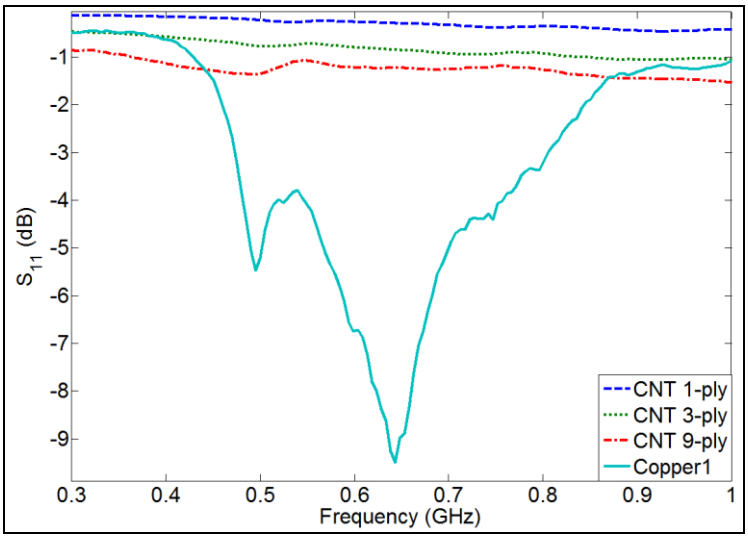

Figure 10. Measured reflection coefficient for 5-in CNT thread/rope and copper stub antennas.

The expected center frequency for each of these antennas was ~2.36 GHz and 590 MHz for the 1.25- and 5-in stub antennas, respectively. A solid resonance is observed for each of the copper stub antennas, as expected; however, no significant resonance is observed for any of the CNT thread stub antennas. These results may be due to a poor electrical connection between the SMA connector and the CNT threads using the silver paste/copper wire fabrication approach. Additionally, the connecting silver paste blobs and connecting wires themselves may have been too large in comparison with the CNT thread (only ~25–75 µm in diameter) and consequently dominated the radiation performance. These results were not successful enough to warrant radiation pattern measurements, and as such, different antenna geometries and feeding

mechanisms were explored. Much better success was achieved with the CNT thread loop antenna and CNT sheet patch antenna prototypes constructed and described in sections 3.1.2 and 3.3.

3.1.2 CNT Thread Loop Antenna

Using samples of the 1-ply CNT thread developed for the dipole antennas in section 3.1.1, a 6.125-in-diameter CNT thread loop antenna was constructed, as shown in figure 11. The CNT thread was passed through a rubber insulator sleeve in order to protect the thread and form the loop shape. This rubber sleeve also fit over the center conductor of the SMA connector and facilitated the process of making an electrical connection between the CNT thread and the connector using only silver paste and without the need for a small segment of copper wire as a bridge.

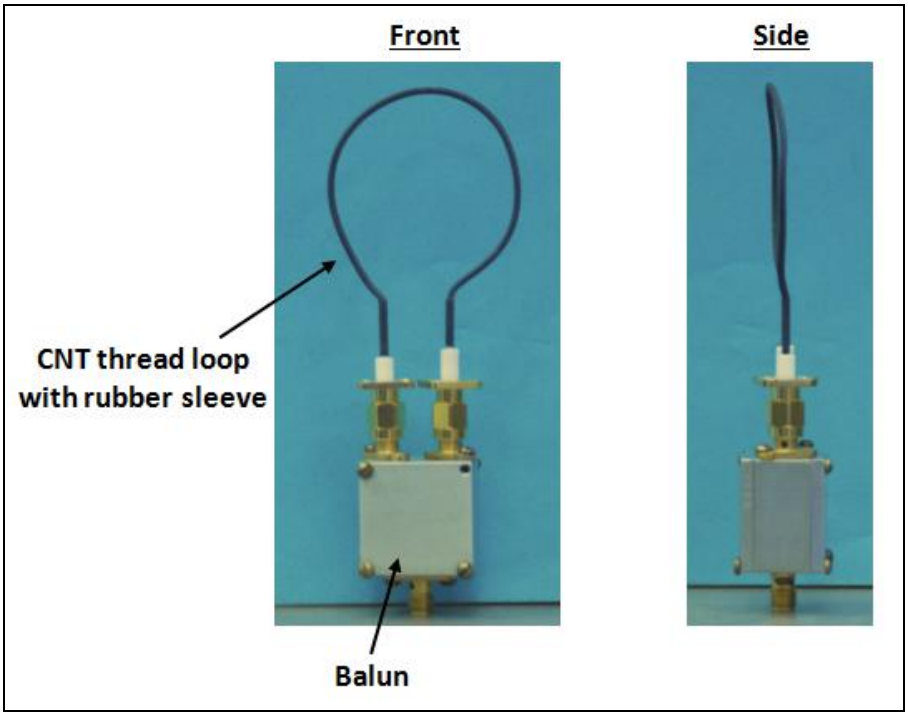

Figure 11. The 5-in-diameter CNT thread loop antenna prototype.

The measure reflection coefficient for this CNT loop antenna is shown in figure 12. A clear resonance is observed at its predicted center frequency of ~1.9 GHz. This result was promising enough to proceed with radiation pattern measurements in the ARL anechoic chamber.

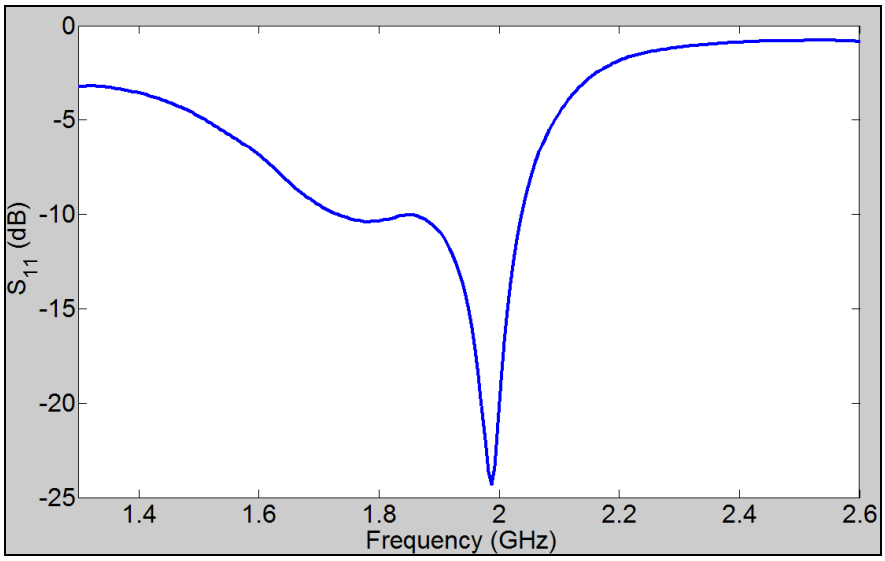

Figure 12. Measured reflection coefficient for CNT thread loop antenna.

The measured radiation patterns for this CNT loop antenna are shown in figures 13 and 14. A reasonable omnidirectional pattern is observed for the azimuth plane radiation pattern, with moderate perturbations observed at certain points. These may be due to the balun/metal enclosure attached to the bottom of the antenna that was of comparable size to the loop. Minor perturbations may also be due to the imperfection of the loop geometry, which was asymmetric and not a perfectly circular shape. The elevation plane radiation pattern also produced reasonable results, with pattern maximums at approximately 90° and 270° and significant pattern drops (~28 dB) at approximately 0° and 180°. The successful performance of the loop antenna prototype compared with that of the dipole antenna prototypes was mainly attributed to the exclusion of the small copper wire bridge that was incorporated at the feedpoint for the dipole antennas. By making a direct connection between the SMA connector to the CNT thread loop antenna structure, the risk that any large-diameter metallic bridge material would dominate the radiation performance was removed.

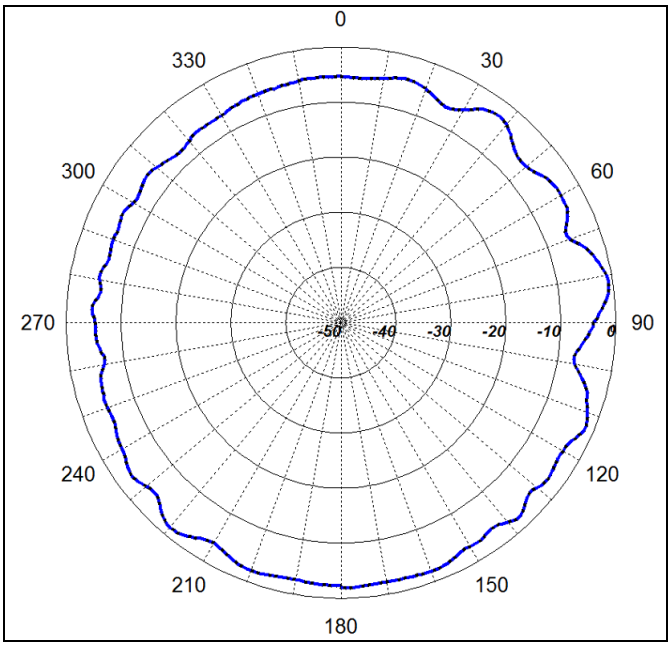

Figure 13. Measured azimuth-plane radiation pattern for the CNT thread loop antenna.

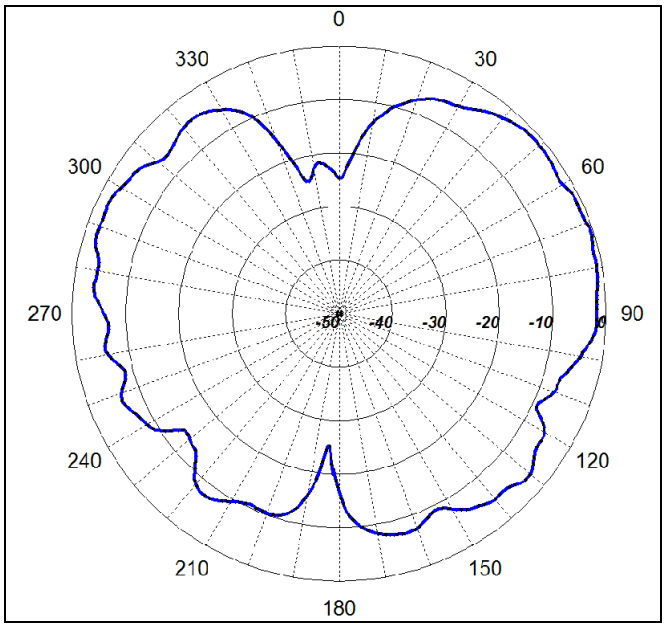

Figure 14. Measured elevation-plane radiation pattern for the CNT thread loop antenna.

3.2 Carbon Nanotube Sheet Antennas

3.2.1 CNT Sheet Fabrication

By modifying the technique employed to fabricate the CNT thread described in section 3.1, it is possible to produce CNT sheet/ribbon materials for planar antenna designs. When the MWNTs

are drawn away from their initial Si substrate, a twisting motion is applied to produce CNT thread, with the van der Waals forces between neighboring CNTs serving as the main binding mechanism. If the twisting motion is removed, it is possible to produce a CNT sheet that is initially the same width as the CNT forest from which the MWNTs are drawn. The width and thickness of this CNT sheet may be adjusted by collecting the sheet on a revolving substrate conveyor belt (e.g., Teflon belt), as shown in figure 15 (*12*). SEM images of the fully fabricated CNT sheet material are shown in figure 16. When the desired width and thickness is achieved, the finalized CNT sheet may then be removed from the initial substrate laminated and/or transferred to a different, preferred substrate. Average thickness for one layer of CNT sheet material is ~50 nm. Practical CNT sheets are at least 10 times this thickness, ranging from 0.5–5 μm.

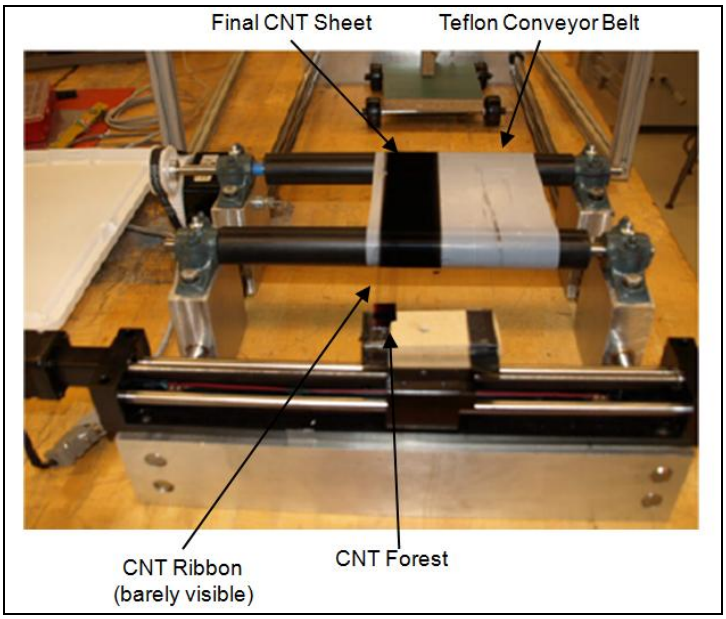

Figure 15. CNT sheet fabrication setup (adapted from reference 11).

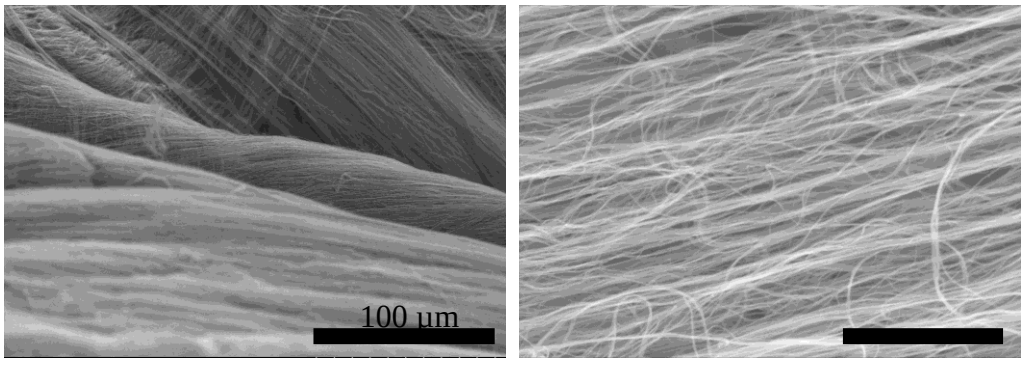

Figure 16. SEM images of fully fabricated CNT sheet.

3.2.2 CNT Sheet Patch Antenna

The measured results obtained from the CNT thread dipole and loop antennas described in section 3.1 were hindered by potential balun radiation and feedpoint connection issues. Thus, it was not possible to make an unbiased comparison between the radiation properties of a CNT material antenna versus that of an antenna fabricated from a standard conductor such as copper using these results.

As an alternative antenna geometry, the aperture-coupled patch antenna, shown in figure 17, was selected due to its indirect feeding mechanism by which a microstrip feedline on the bottom surface of a lower substrate couples an applied signal up through an aperture located in a ground plane on the bottom surface of an upper substrate to a radiating patch located on the top surface.

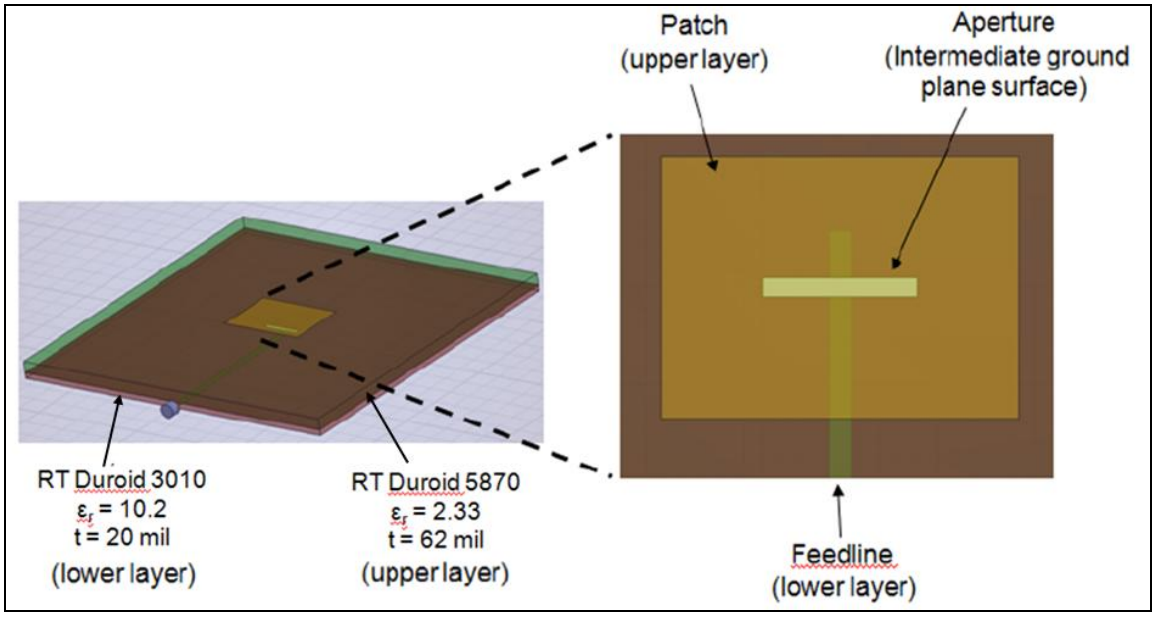

Figure 17. X-band aperture-coupled patch antenna design.

A standard X-band aperture-coupled patch antenna design, previously developed for the ARL Compact Radar (*12*), was employed for this experiment. CNT sheet material was fabricated at the University of Cincinnati and transferred to a Kapton tape substrate, which provided both an adhesive bonding mechanism on one side and a lamination protective mechanism on the other. This Kapton-laminated CNT sheet was then affixed to the top surface of a 62-mil RT/Duroid 5870 dielectric board (the patch layer substrate for the design), as shown in figure 18, and cut to the precise patch antenna dimensions using an in-house circuit board router at ARL. A version of this patch was also constructed from standard copper-clad RT/Duroid 5870 material.

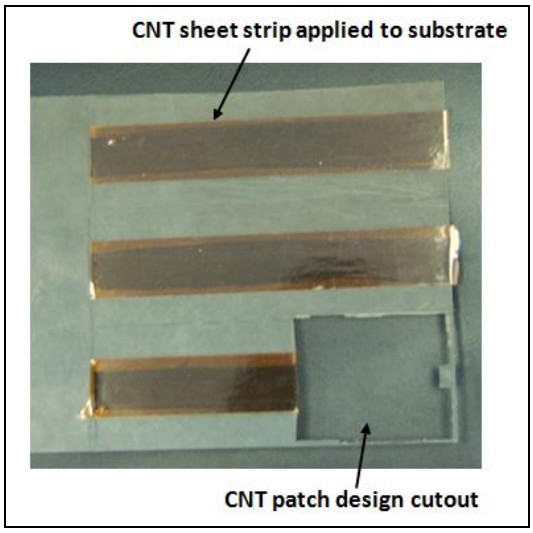

Figure 18. CNT sheet material/Kapton tape applied to RT/Duroid 5870 substrate.

The microstrip feedline and ground plane layers were fabricated from standard copper for all prototypes. By keeping all design dimensions and materials the same except for the patch material and by employing an indirect feeding mechanism to the patch, it was possible to make a direct comparison between the radiating properties of the CNT sheet material versus that of standard copper cladding. The fully fabricated patch antenna prototypes are shown in figure 19.

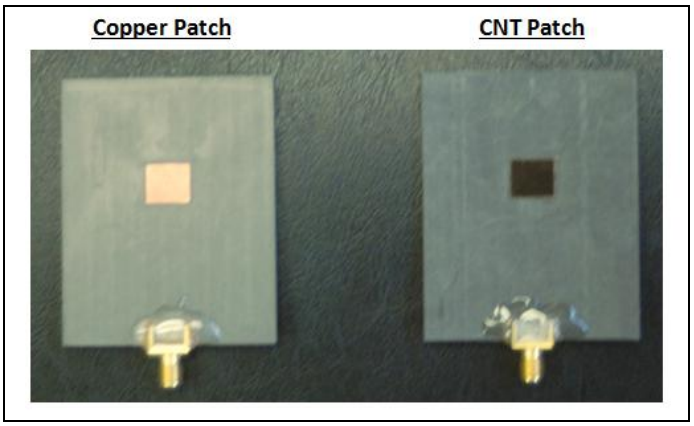

Figure 19. Copper and CNT sheet aperture-coupled patch antenna prototypes.

Full-wave electromagnetic simulations of this patch antenna design were conducted using *Ansoft* High Frequency Structure Simulator (HFSS) prior to fabrication. For the initial comparison, a 0.5-μm-thick CNT sheet (~10 layers of CNT sheet material) and a 5-μm-thick CNT sheet (~100 layers of CNT sheet material) were used to fabricate the CNT sheet patch antenna prototypes. The estimated thickness for the 0.5-oz copper coating used on the RT/Duroid board for the copper patch antenna prototype was ~17 μm. The CNT sheet patch was approximated as a finite conductivity boundary in the simulation. The conductivity of this boundary was estimated to be

~3e4 S/m from the measurements conducted in year 1 of the DRI on the CNT thread material. The actual conductivity of the CNT sheet material may be significantly higher than that of the CNT thread and can likely be improved to at least 1e5 to 1e6 S/m with post-processing techniques. The finite conductivity boundary was placed in between two layers of 5-mil-thick Kapton film in order to represent the Kapton laminate/bonding layers on the actual prototype. This film had an estimated permittivity of $\varepsilon_r = 3.5$. The effects of CNT sheet thickness and conductivity on patch antenna radiation performance were explored, as shown in figure 20.

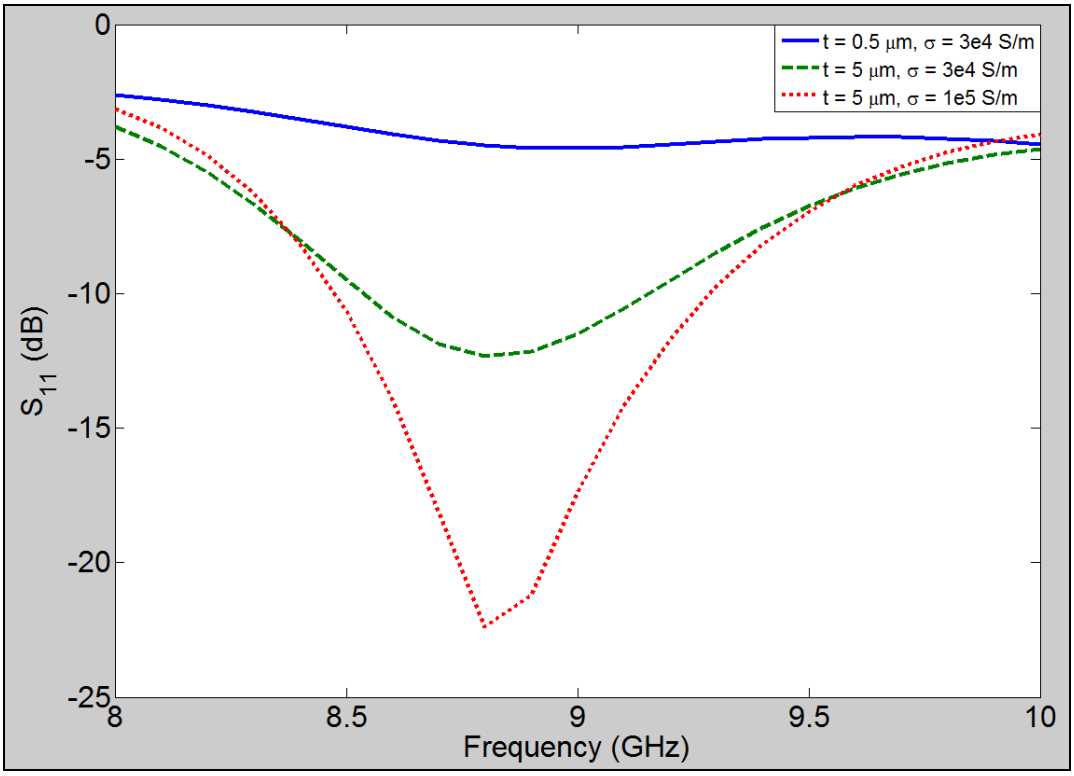

Figure 20. Effect of CNT sheet thickness and conductivity on reflection coefficient for CNT sheet patch antennas.

The high predicted reflection coefficient (and subsequently poor radiation performance) for the 0.5-μm-thick CNT sheet patch antenna was suspected to be due to the fact that the thickness was much smaller than the skin depth of the material at 9 GHz. The skin depth represents the distance that an electromagnetic wave penetrates beneath the exterior surface of a conductor, since that is where the current density is largest, and is calculated as

$$\delta_s = \sqrt{\frac{2\rho}{\omega\mu}} \tag{1}$$

where ρ is the material resistivity, ω is the angular frequency, and μ is the material permeability. For an estimated conductivity of ~3e4 S/m, frequency of 9 GHz, and estimated permeability of 4πe-7 H/m, the skin depth for the CNT sheet material is estimated to be $\delta_s \approx 30$ μm. This is

higher than the 0.7-µm skin depth estimated for a copper sheet, due to its conductivity of ~5.9e7 S/m. A significant improvement in the reflection coefficient is predicted when the CNT sheet thickness is increased from 0.5 to 5 µm. An efficient patch antenna with $S_{11} < -10$ dB (less than 10% power reflected back to the RF source) is predicted to be attainable with a 5-µm CNT sheet with conductivity as low as 3e4 S/m. As the conductivity is improved to 1e5 S/m (which is expected to be surpassed with post-processing techniques), a reflection coefficient and bandwidth that rivals a traditional copper patch antenna is predicted. Thus, with reasonable conductivity and by increasing the CNT sheet thickness closer to its estimated skin depth, a significant increase in radiation performance was expected. This was observed in the reflection coefficient measurement results shown in figure 21.

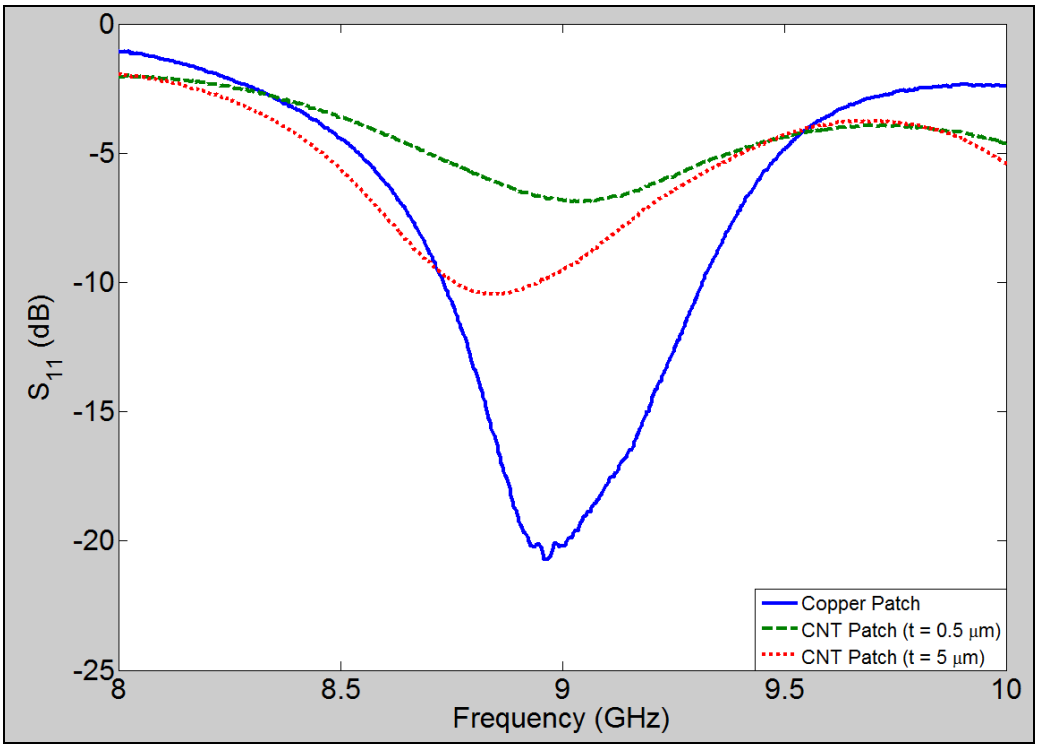

Figure 21. Measured reflection coefficient for CNT sheet and copper patch antenna prototypes.

While the 0.5-µm CNT sheet patch antenna does resonate at ~9 GHz, its reflection coefficient (–6 dB, or 25% power reflected back to RF source) is much higher than that of the standard copper antenna (–21 dB, or 0.8% power reflected back to RF source). The measured input impedance at 9 GHz was ~44 + j8.8 Ω for the copper patch antenna and was ~40.5 + j44 Ω for the 0.5-µm CNT sheet patch antenna. For these measurements, the real part represents the input resistance and the imaginary part represents the input reactance, with a positive value being inductive reactance and a negative value being capacitive reactance. A perfect match to the RF source would be a measurement of 50 + j0 Ω. Both resistance values were close to the desired 50 Ω, though the inductive reactance value for the CNT sheet patch was ~5 times higher than that of the copper patch.

A significant performance improvement was observed for the 5-µm CNT sheet patch antenna, with a –10.5-dB reflection coefficient at resonance. A minor resonant frequency shift of ~100 MHz (~1.5%) from 9 to 8.85 GHz was observed, potentially due to increased reactance from the CNT sheet layers and/or from fabrication tolerance errors. The measured input impedance at resonance was ~75 + j28 Ω. Thus, while the increased CNT sheet thickness did lower the reactance component of the input impedance, the resistance component was increased and the overall reflection coefficient remained well above that of the copper patch antenna. It should be noted that a 5-µm sheet thickness was still well below the skin depth of ~30 µm for a 3e4 S/m conductor. In order to surpass the skin depth, a CNT sheet composed of ~600 layers of CNT sheet material would be needed. If the CNT sheet conductivity can be improved, the skin depth will decrease and the required number of CNT sheet layers will also decrease. While the simulations had predicted a ~6.5% to 7% bandwidth (~600 MHz) of $S_{11} < -10$ dB for this antenna, the measured prototype exhibited only a 2.3% bandwidth (~200 MHz) due to the reflection coefficient just barely passing below –10 dB. If the reflection coefficient improves with increased conductivity as the simulation results in figure 21 indicate, the bandwidth will also increase for a future optimized design.

When the CNT sheet material is fabricated by pulling CNTs from a MWNT forest along a Teflon belt, the CNTs within the sheet bind together and are oriented in approximate alignment with the direction that the CNTs are pulled along the belt. Since electrons travel axially along the CNTs and rarely tunnel between neighboring nanotubes unless there is significant overlap, the RF performance of a CNT sheet patch antenna may be significantly impacted by the orientation of the CNTs within the sheet. For the prototype measured in figure 21, the CNTs within the sheet material were oriented parallel to the E-plane for the patch antenna (along the length of the patch, parallel to the microstrip feedline). A third patch antenna prototype was fabricated with the CNTs oriented orthogonal to the antenna E-plane. This distinction is illustrated in figure 22.

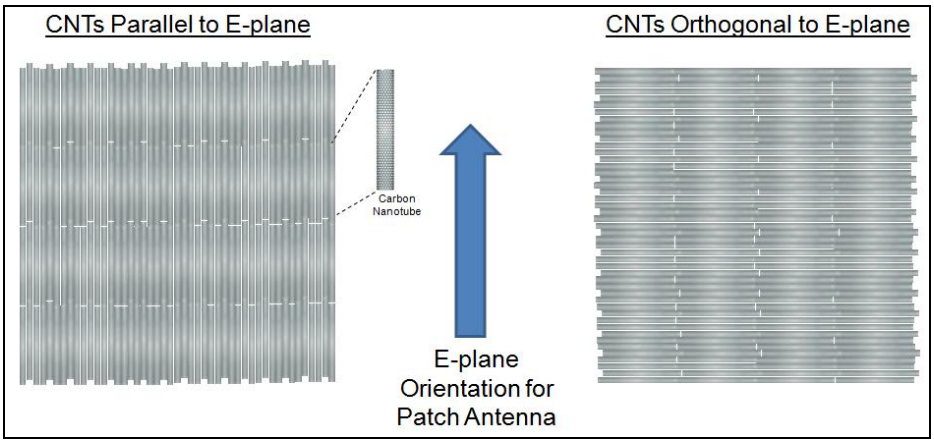

Figure 22. Variation in CNT sheet orientation for CNT sheet patch antenna prototypes.

The effect of CNT orientation on the patch antenna reflection coefficient is shown in figure 23. The reflection coefficient indicates that the orthogonal orientation of the CNT sheet to the

E-plane of the antenna results in significant detuning at the expected resonance of ~8.8 to 9 GHz and a potential resonant frequency shift down to ~8.4 GHz (4–5% shift). The measured input impedance at this shifted resonance was ~68 + j91 Ω. While the resistance component was brought closer to the desired 50 Ω, the inductive reactance component was significantly increased.

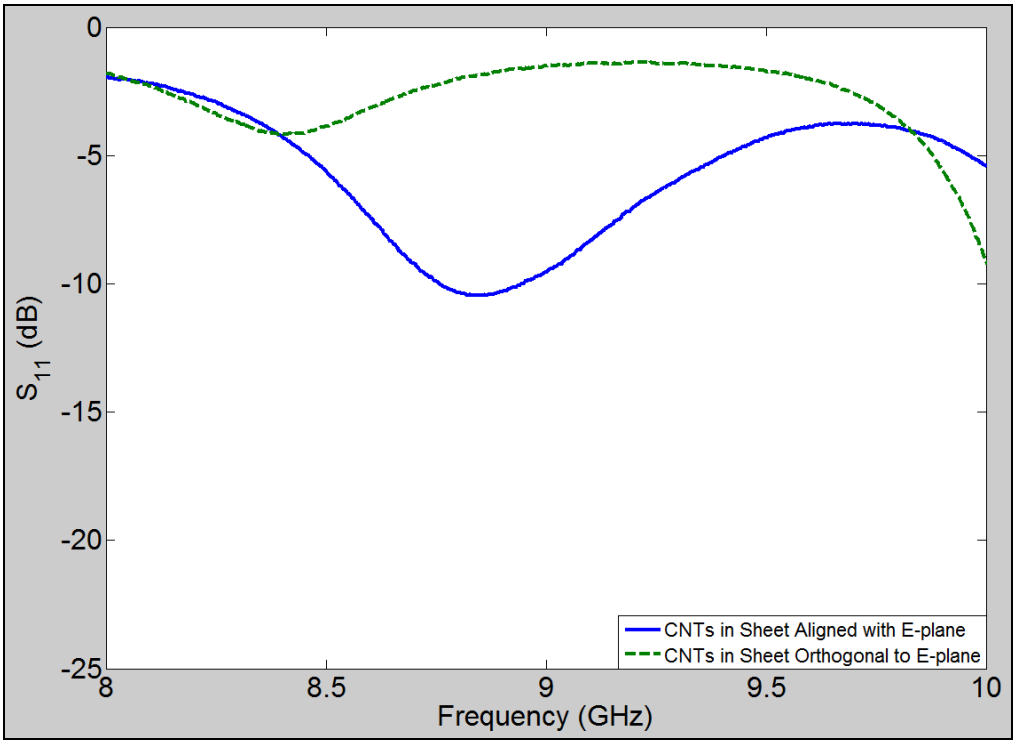

Figure 23. Effect of CNT sheet orientation on measured reflection coefficient for CNT sheet patch antennas.

The measured radiation pattern and gain data for each of the prototypes is shown in figures 24–26. The baseline copper patch antenna and the CNT patch antennas with the CNTs aligned with the E-plane of the patch all displayed a typical patch antenna radiation pattern, with a half-power beamwidth (HPBW) of ~75° to 80° for both the E-plane and H-plane. Minor perturbations in some of the patterns were likely due to measurement error and/or radiation from the feedline and SMA connector feedpoint. The "orthogonal" CNT sheet patch antenna radiation pattern was not consistent between the E- and H-planes and displayed poor performance, as was expected from its previously measured poor reflection coefficient data.

The copper patch antenna displayed a realized gain of ~5.6 dBi, just a little under the theoretical 7 dBi of an ideal patch antenna. The 5-µm "aligned" CNT sheet patch antenna exhibited a realized gain of 2.05 dBi, indicating an ~3.5-dB tradeoff in radiated power for using 5-µm CNT sheet material in place of standard copper for the patch. When the CNT sheet thickness was reduced by 10x to 0.5 µm, a –3.5-dBi realized gain was observed, indicating that this reduction in thickness resulted in a gain reduction of ~9.1 dB from the standard copper patch and ~5.5 dB

from the 5-µm CNT patch antenna. The impact that the CNT sheet orientation has on the radiation performance of the patch antenna is clearly seen with the 5-µm "orthogonal" CNT sheet patch antenna, which exhibited a realized gain of –6.1 dBi. This indicates significant polarization selectivity for the CNT sheet patch antennas, with ~8.2-dB difference in realized gain observed between prototypes constructed with the exact same design and from the exact same batch of CNT sheet material depending on whether the CNTs within the sheet material were generally aligned with the E-plane of the antenna. This behavior may have significant applications to polarization-specific antennas and may be useful for improving isolation between neighboring antennas on Army platforms.

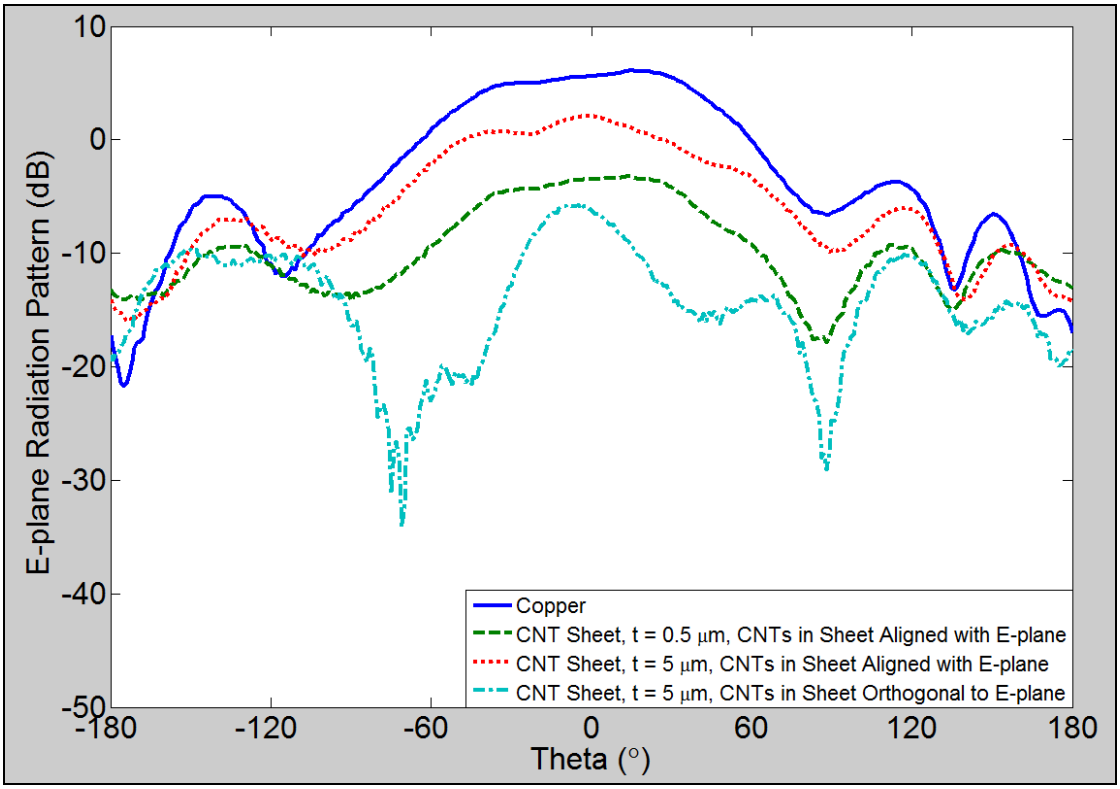

Figure 24. Measured E-plane radiation pattern for CNT sheet and copper patch antenna prototypes.

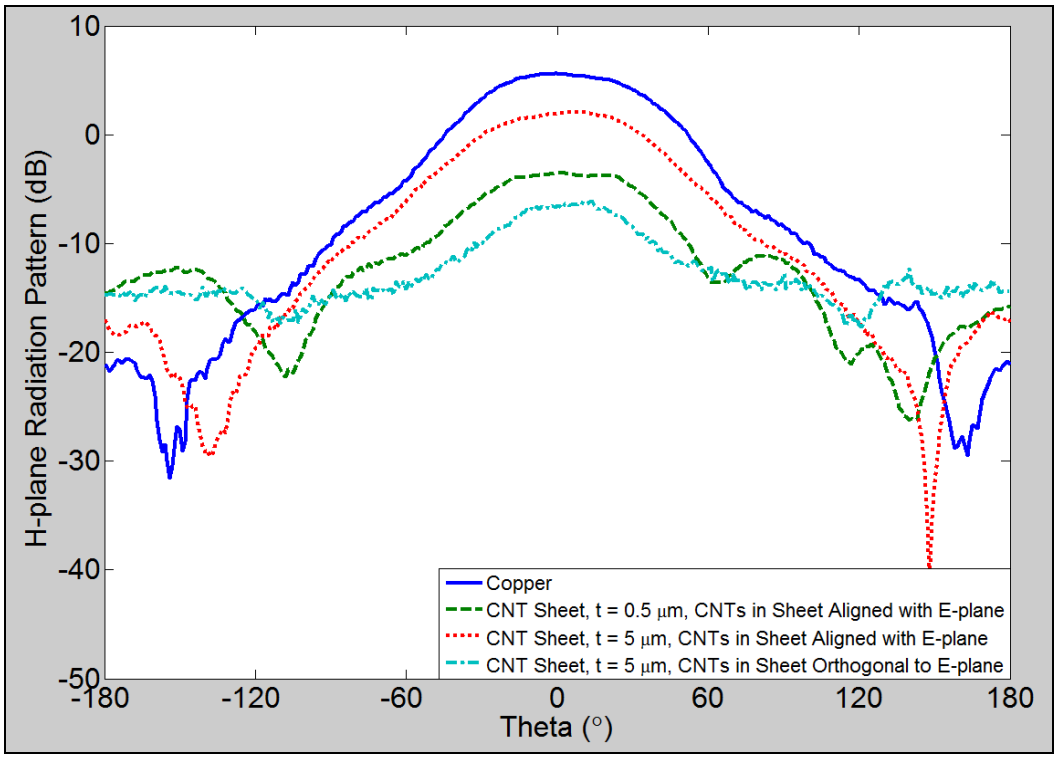

Figure 25. Measured H-plane radiation pattern for CNT sheet and copper patch antenna prototypes.

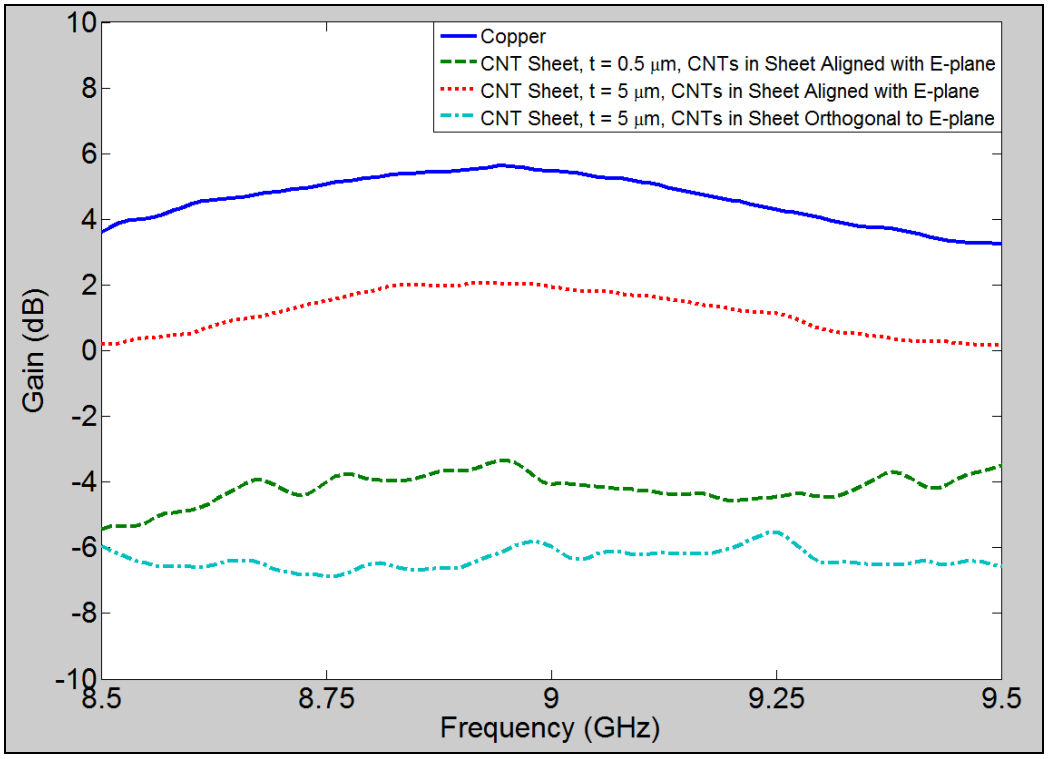

Figure 26. Measured realized gain for CNT sheet and copper patch antenna prototypes.

3.3 Meshed Carbon Nanotube Thread Patch Antenna/Gas Sensor

3.3.1 Design and Simulation

Recent research has shown that the permittivity, ε_r, and conductivity, σ, of a CNT is temporarily altered when it is subjected to certain gases, especially oxidizing/reducing gases such as ammonia (NH_3) and oxygen (O_2) (*13*). This reaction has been exploited as a gas sensor by incorporating a thin layer of either randomly scattered SWNTs (*14–17*) or aligned MWNTs (*18*) as part of a microwave resonator. The resonator center frequency shifts in direct response to the change in the permittivity of the CNT layer that occurs due to the presence of a reacting gas. While the mechanism by which this permittivity shift occurs has not been conclusively determined, it is generally accepted that this shift arises from charge transfer between the reacting gas molecules and the nanotubes, with the molecules acting as either electron donors or acceptors (*19*). All of these unique properties may be exploited in the proposed meshed CNT thread patch antenna to provide a multifunctional communications/gas sensor system that can be fully integrated into a textile substrate.

The patch antenna has proven to be quite effective for a variety of applications, including terrestrial and satellite communications systems and various radar electronic scanning arrays due to its low-profile, planar structure, reasonable bandwidth of typically 10%–20%, and excellent gain of typically 7 dBi. Previous research has shown that substituting a meshed conductive structure for the radiating patch and/or ground plane in place of a traditionally used solid conductive structure (e.g., copper, CNT sheet) yields no significant change to the antenna radiation pattern and moderate losses in gain and bandwidth depending on the density of the mesh (*20*). By applying interwoven CNT thread/rope to such a design, it may be possible to construct a patch antenna capable of being easily integrated into a textile material for applications in which weight, flexibility, and durability are major concerns.

A basic aperture-coupled microstrip fed patch antenna was designed to provide a layout for the meshed CNT thread patch antenna. The baseline solid metal patch antenna was designed to operate at K_a-band in order to allow for future SATCOM applications and also to keep the patch dimensions small enough for the simulation of the meshed patch antenna, composed of individual CNT threads with μm radius. The specific center frequency of the basic solid metal patch design was f_0 = 30 GHz, but a downward frequency shift was expected in the final meshed CNT thread antenna due to the meshed thread structure and the dielectric-loading semiconducting CNT spacer threads.

A model of the meshed CNT thread patch antenna is shown in figure 27. The antenna consists of a 2.7 x 3.7 mm patch constructed from 25-μm-diameter meshed CNT threads residing on a dielectric substrate and fed with aperture coupling by a 50-Ω microstrip feedline (w = 239 μm). While the ultimate goal is for this design to be fully embedded in a flexible, body-wearable textile substrate, the substrate used for this initial proof of concept is RT/Duroid 6010 (ε_r = 10.2, t = 10 mil) for the feedline layer and RT/Duroid 5870 (ε_r = 2.33, t = 20 mil) for the patch layer,

with a metallic ground plane and aperture (l = 1587 μm, w = 190 μm) separating the two layers. In order to achieve multifunctionality, the CNT threads that comprise the meshed patch are alternated between fully conducting thread fabricated from MWNTs and semiconducting threads fabricated using the same technique but with a significant number of defects added, as shown in figure 28. The additional defects introduced to the semiconducting threads ensure that the threads exhibit lower conductivity than their conductive thread neighbors (closer to a dielectric buffer) and also provide more locations for reactive gas molecules to donate or accept electrons, thus increasing the likelihood that a reactive gas will cause a noticeable change in the thread permittivity. The threads were spaced ~λ/67 apart.

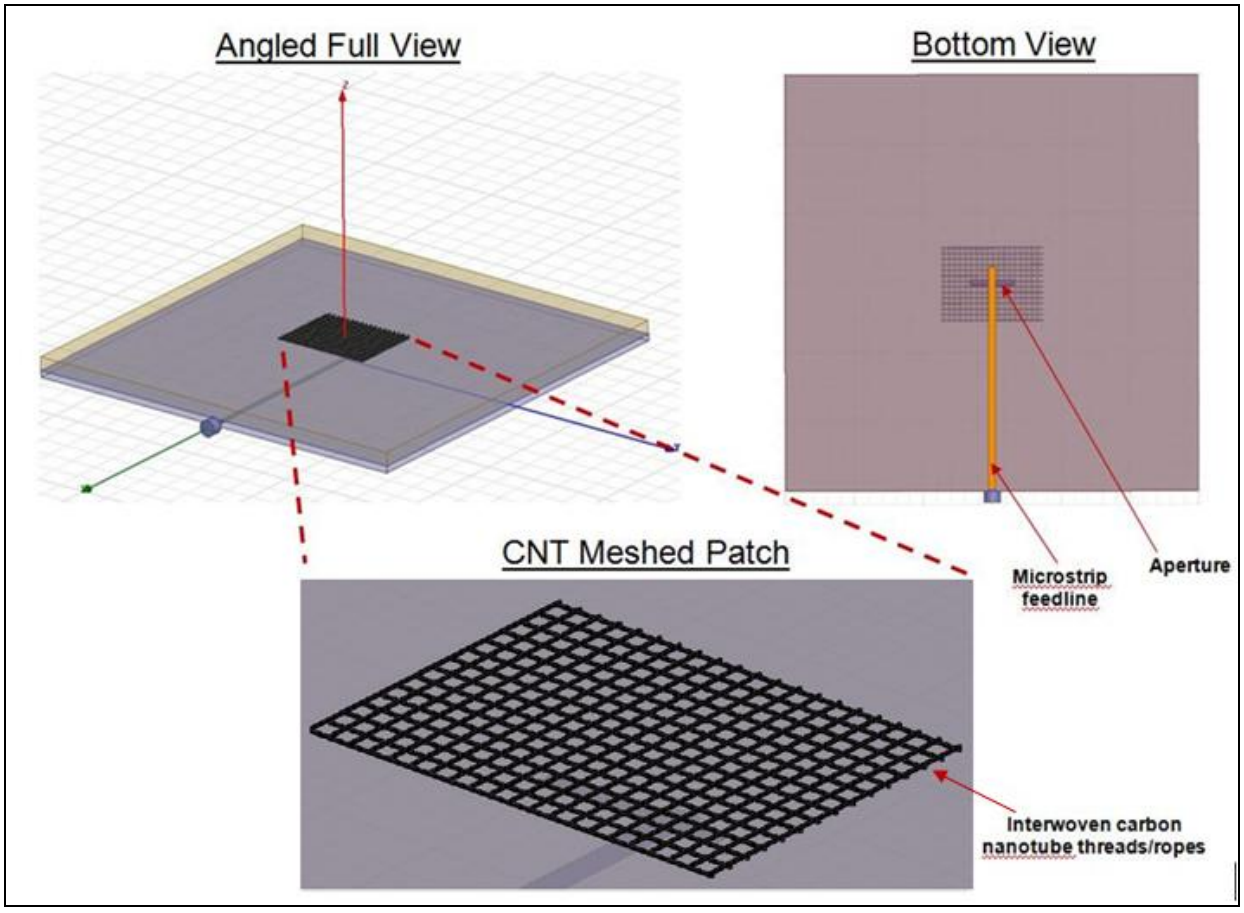

Figure 27. Model of meshed CNT thread patch antenna.

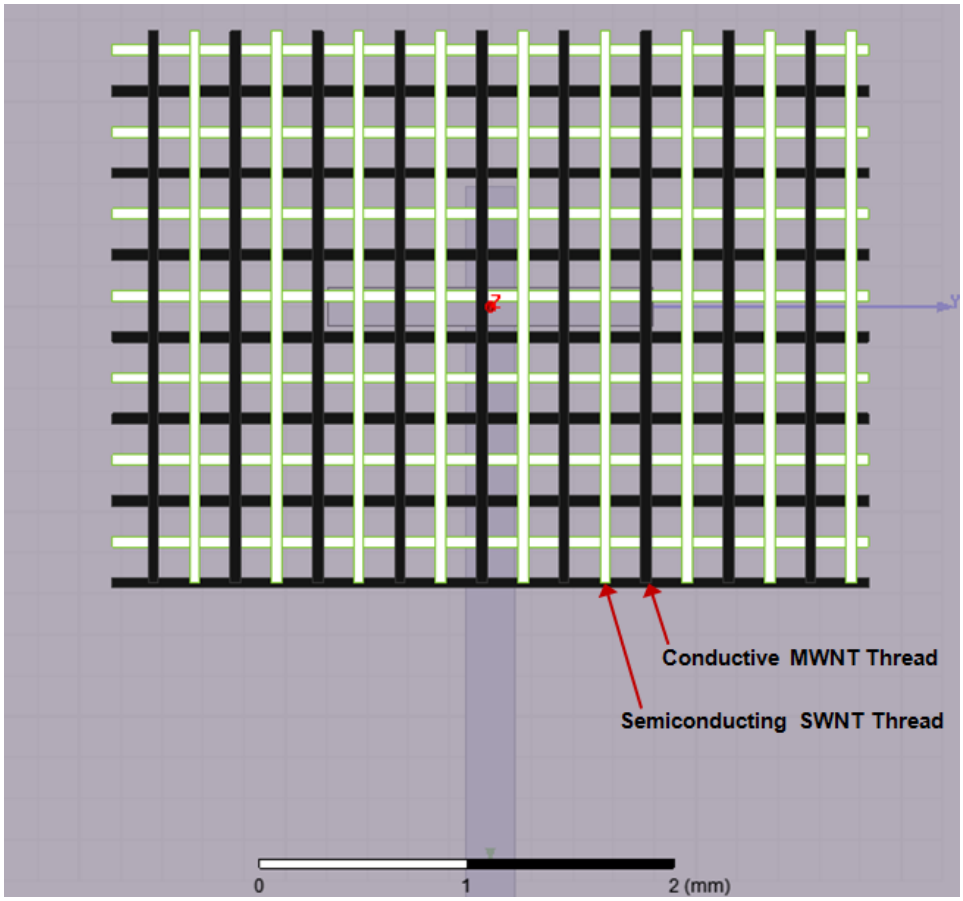

Figure 28. Model of patch antenna/gas sensor fabricated from meshed conductive and semiconducting MWNT thread.

With the conductive CNT threads serving as the meshed patch antenna structure and the semiconducting CNT threads serving as dielectric spacer material with variable permittivity based on the presence of a reacting gas, this meshed CNT thread patch may simultaneously serve as both the radiating antenna for a communications system and as the dielectric loaded resonator for a gas sensor system.

Based on measured data, the conductive threads were modeled in Ansoft HFSS as rectangular tubes with σ = 1e6 S/m (*21*) while the semiconducting threads were modeled as material with estimated ε_r = 5 (*18*). It should be noted that this full wave simulation does not account for defects in the CNT walls that may disrupt electron flow and act as a resistive barrier. Also unaccounted for are quantum-level effects such as the quantum capacitance and kinetic inductance for the individual CNTs that comprise the threads. Each of these factors will likely increase the total resistance of the CNT thread and thus decrease the overall conductivity. An initial simulation was conducted to predict the change in f_0 expected for the meshed CNT thread patch antenna in the presence of a reacting gas. The antenna exhibits a center frequency, f_0 = 27.85 GHz, and –10 dB bandwidth of 2.1 GHz. This is a center frequency shift of ~2 GHz (7%) and bandwidth reduction of ~400 MHz (16%) from the center frequency of 29.6 GHz and

–10 dB bandwidth of 2.5 GHz predicted for the baseline solid patch antenna, as shown in figure 29. The simulated realized gain for the meshed CNT thread patch antenna is shown in figure 30. The peak total realized gain ($\phi = 0°$, $\theta = 90°$) was predicted to drop ~0.46 dB (7%) from 6.79 to 6.33 dB by substituting the meshed CNT thread patch for the baseline solid copper patch.

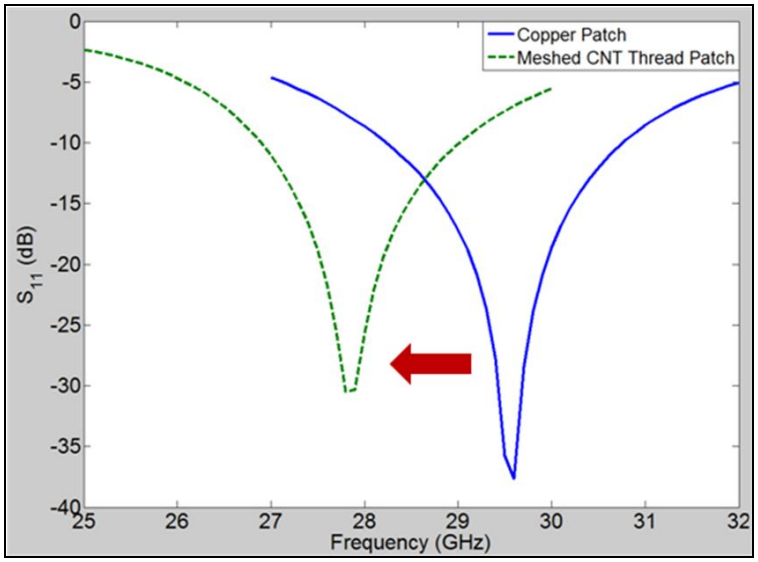

Figure 29. Simulated reflection coefficient for meshed CNT thread patch antenna.

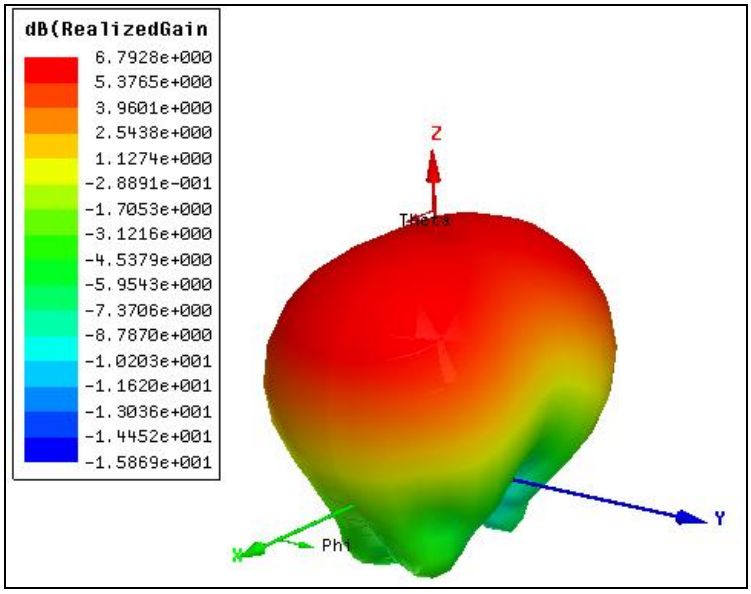

Figure 30. Simulated realized gain (three-dimensional [3-D] polar plot) for meshed CNT thread patch antenna.

In addition to operating as a radiating antenna for communications applications, the meshed CNT thread patch may also serve as a resonator for a gas sensor system. Previous research has shown through measurement that ε_r for a thin layer of mainly semiconducting SWNTs increases linearly

when in the presence of increasing concentrations of NH_3 (*18*). The estimated changes in ε_r from these measurements for NH_3 concentrations is an approximate increase from $\varepsilon_r = 5$ to $\varepsilon_r = 5.15$ for 1000 ppm and increases of 0.15 with each additional 3000 ppm. These varying permittivity values were applied to the semiconducting CNT threads in the HFSS model of the meshed CNT thread patch antenna and the resulting shifted f_0 was simulated, as shown in figure 31. A small but measurable resonant frequency shift of –60 MHz is predicted to occur as the concentration of NH_3 is increased around the meshed patch antenna. This shift in f_0 is large enough to measure with the appropriate complementing gas sensor circuitry and small enough to guarantee continuous bandwidth for communications functionality.

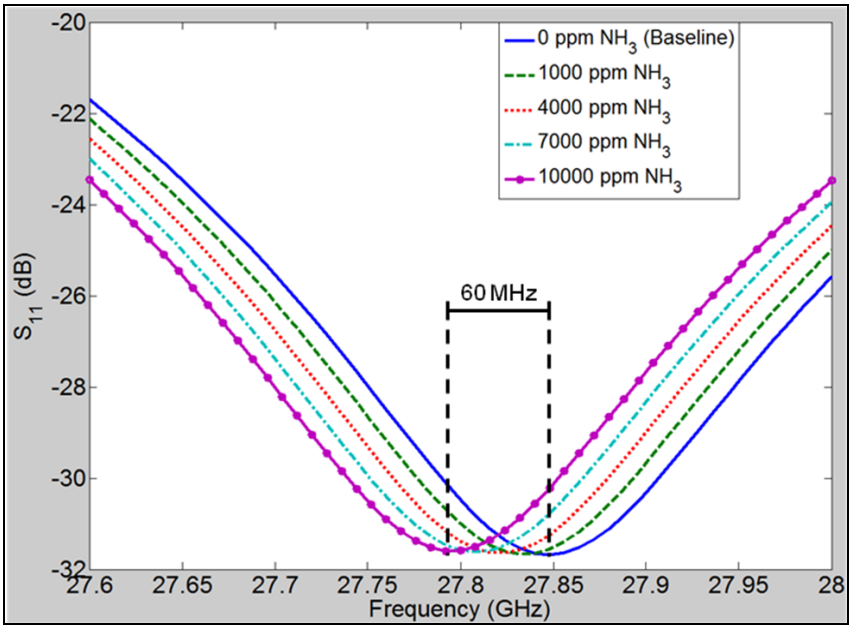

Figure 31. Simulated change in meshed CNT thread patch antenna resonant frequency in presence of varying concentrations of NH_3 gas.

It is important to note that RT/Duroid materials were used as the antenna substrate for this study mainly due to their low-loss nature and their well-defined permittivity values since the focus of the study was on the meshed thread spacing and the viability of its use as the feedline and/or ground plane. This specific design is not flexible and would not be a practical application of the meshed CNT thread materials. A future embodiment of this concept will employ one or more fabric materials as the antenna substrates in order to facilitate the integration of the meshed CNT thread patch antenna/gas sensor into a high-durability, lightweight body-wearable system.

3.3.2 CNT Thread Spacing/Meshed Thread Feedline and Ground Plane Viability

Follow-up simulations were conducted to understand the impact that CNT thread spacing would have on the meshed patch antenna performance and assess the viability of fabricating other parts of the patch antenna (feedline, ground plane, etc.) from the meshed CNT thread material. Figure 32 details the $\lambda/60$ and $\lambda/15$ models of the thread spacing study that was conducted. For

these simulations, the feedline and ground (GND) plane were modeled as ideal perfect electric conducting (PEC) surfaces.

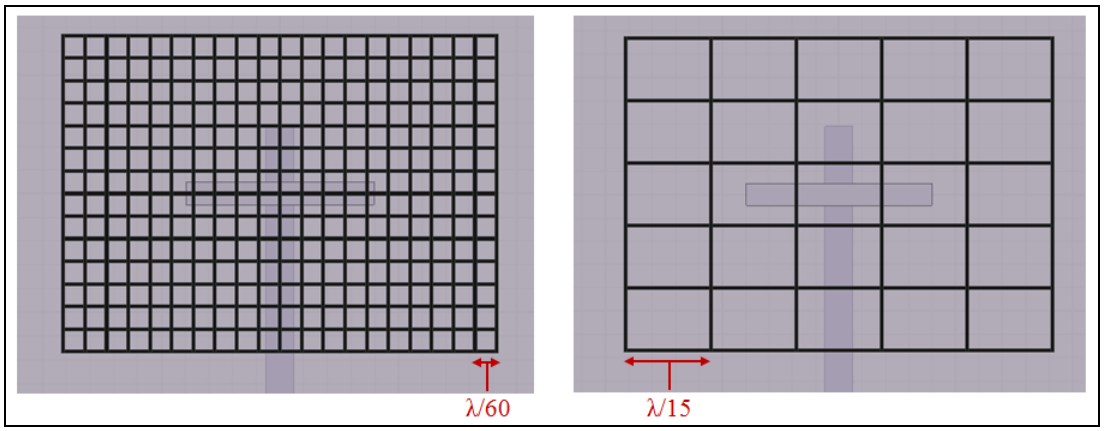

Figure 32. Meshed CNT thread spacing variation.

The borders of the meshed thread patch were kept constant and centered over the aperture/feedline as the spacing between neighboring CNT threads was adjusted from λ/60 to λ/15. Since the patch dimensions remained fixed, the density of the meshed CNT thread within the patch antenna area decreased as the thread spacing was increased. Simulations were conducted to examine the reflection coefficient, realized gain, and bandwidth of the antenna. The surfaces of each CNT thread were approximated as finite conductivity boundaries with their conductivity set to the previously measured value of ~3e4 S/m. The results for these simulations are detailed in figures 33–37.

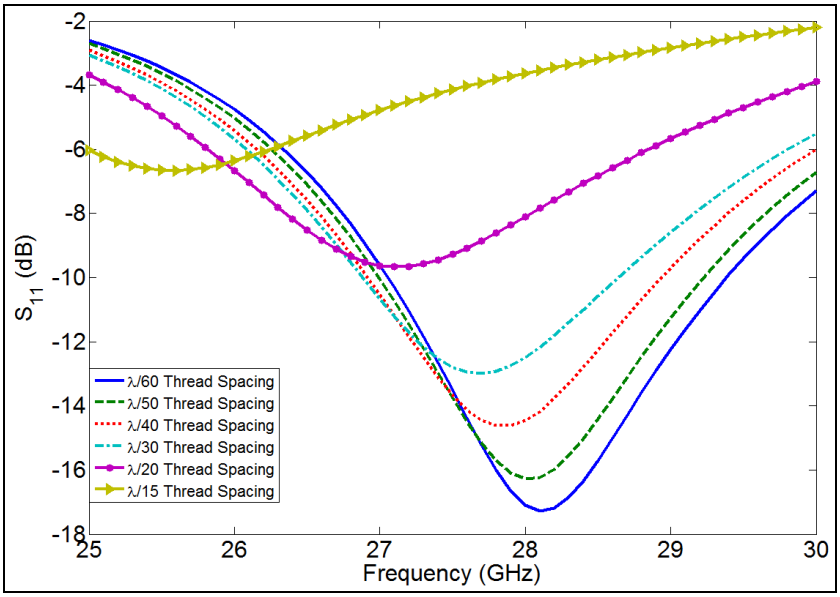

Figure 33. Effect of thread spacing on reflection coefficient for meshed CNT thread patch antennas.

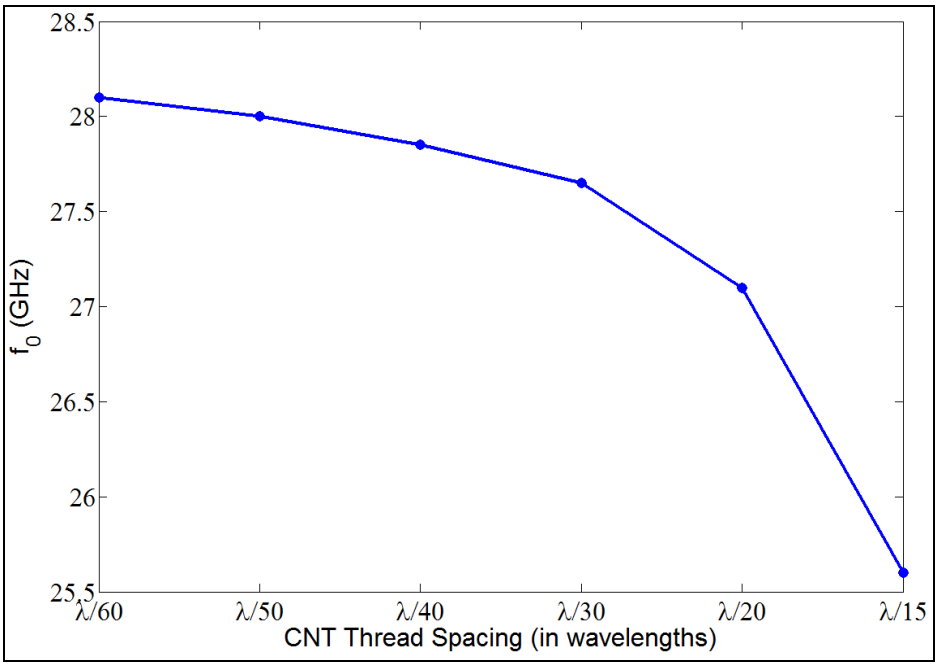

Figure 34. Effect of thread spacing on center frequency for meshed CNT thread patch antennas.

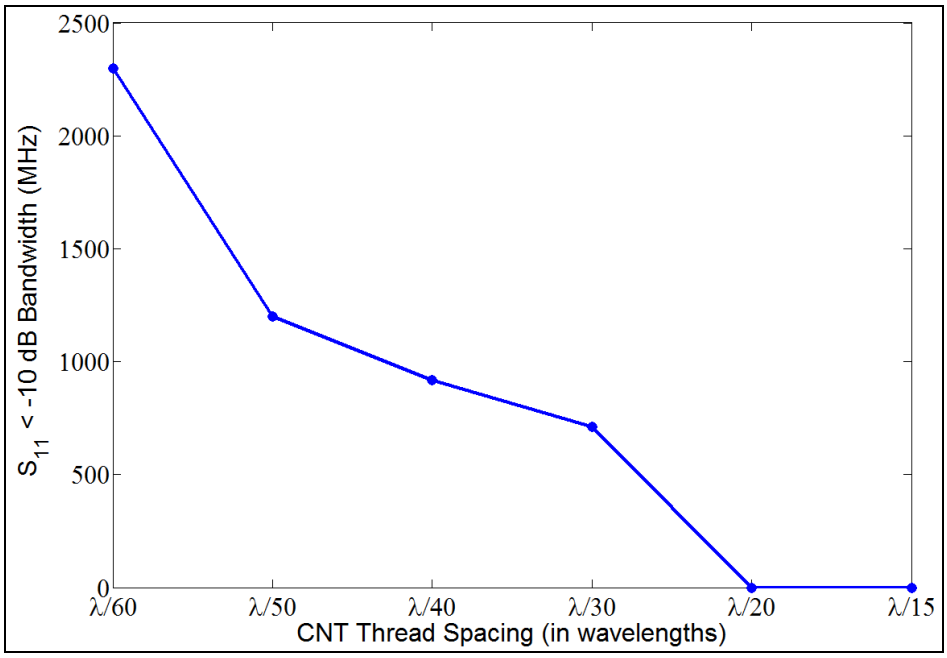

Figure 35. Effect of thread spacing on bandwidth for meshed CNT thread patch antennas.

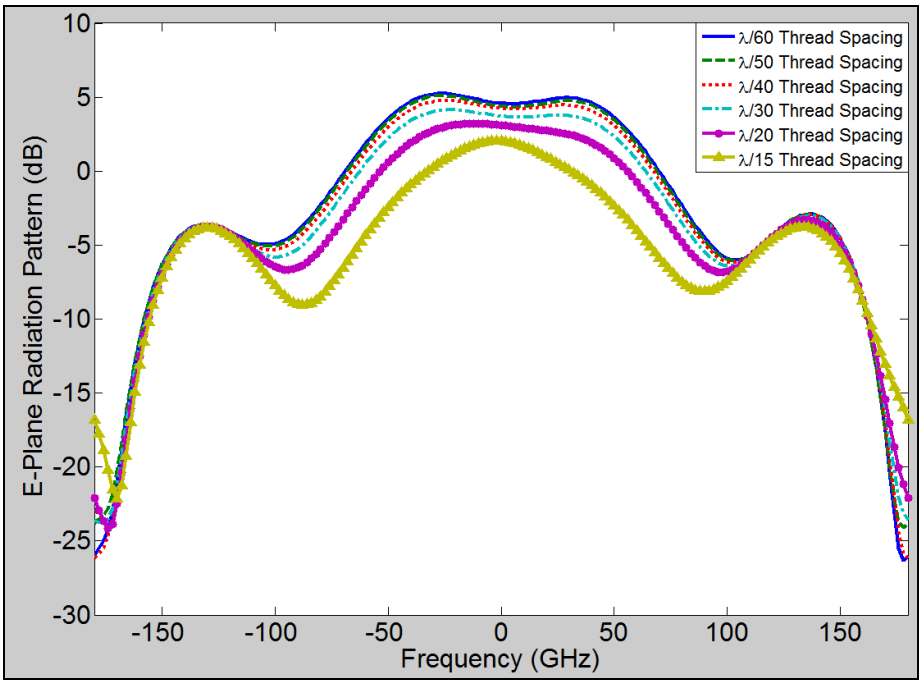

Figure 36. Effect of thread spacing on radiation pattern for meshed CNT thread patch antennas.

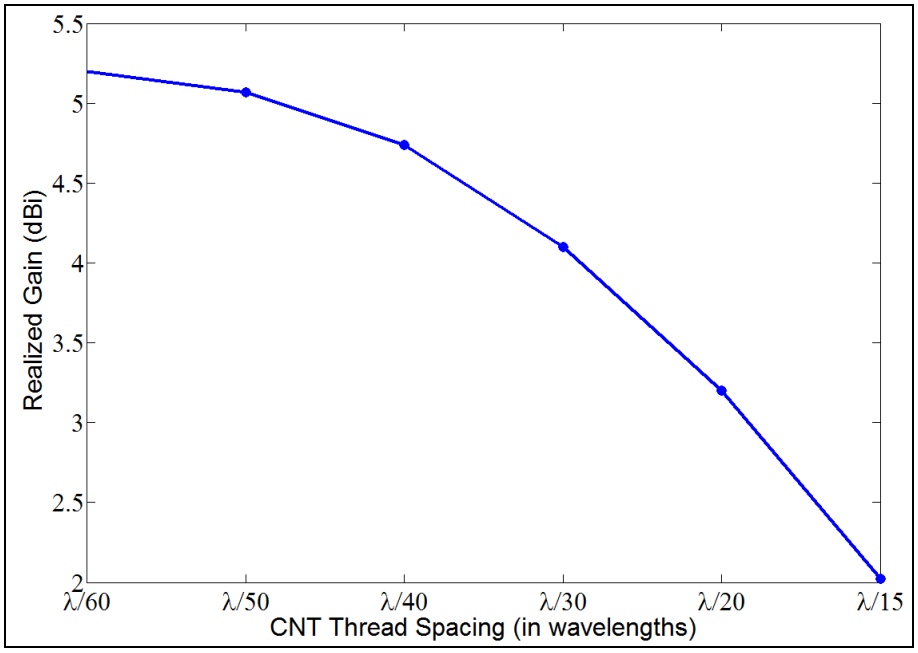

Figure 37. Effect of thread spacing on realized gain for meshed CNT thread patch antennas.

As the thread spacing is increased, the patch antenna experiences a center frequency shift from ~28.1 GHz with λ/60 spacing to ~25.6 GHz with λ/15 spacing (8.9% shift). The $S_{11} < -10$ dB bandwidth decreases as this frequency shift occurs, from ~2.3 GHz at λ/60 spacing to 0.71 GHz at λ/30 spacing (70% reduction). As the spacing is increased beyond λ/30, the bandwidth with $S_{11} < -10$ dB disappears completely, indicating that the antenna radiation efficiency will be severely reduced.

From the E-plane radiation pattern plot shown in figure 36, the HPBW is shown to remain relatively steady at ~120° for λ/60 through λ/30 spacing and then sharply declines as the spacing is increased further, being ~100° at λ/20 spacing and 80° at λ/15 spacing. The realized gain also drops from ~5.2 dBi with λ /60 spacing to ~2 dBi with λ/15 spacing. This is likely due to the impedance mismatch that is reflected in figure 33, which shows that the S_{11} value at resonance increases as the thread spacing increases, from a minimum of –17.3 dB with λ/60 spacing to a minimum of –6.7 dB with λ/15 spacing.

The data from these simulations indicate that a thread spacing of $d \leq \lambda/30$ will ensure sufficient antenna radiation efficiency and usable bandwidth, with the caveat that antenna bandwidth will shrink as the thread spacing is increased. The minor center frequency shift and gain reduction will also need to be accounted for in the design process when the thread spacing is increased.

Simulations were also conducted to investigate the viability of constructing the antenna feedline and ground plane from the meshed CNT thread material. For each of these cases, the CNT thread spacing was set to λ/60. An electromagnetic model of the patch antenna with the feedline, ground plane and patch all composed of meshed CNT thread is shown in figures 38 and 39. In order to accurately realize the dimensions and location of the aperture for the antenna, the density of the meshed CNT threads composing the ground plane layer was increased for the area near the aperture, with a thread spacing of ~λ/120. This spacing was also used for the threads composing the feedline layer in the longitudinal direction in order to accurately realize the feedline width.

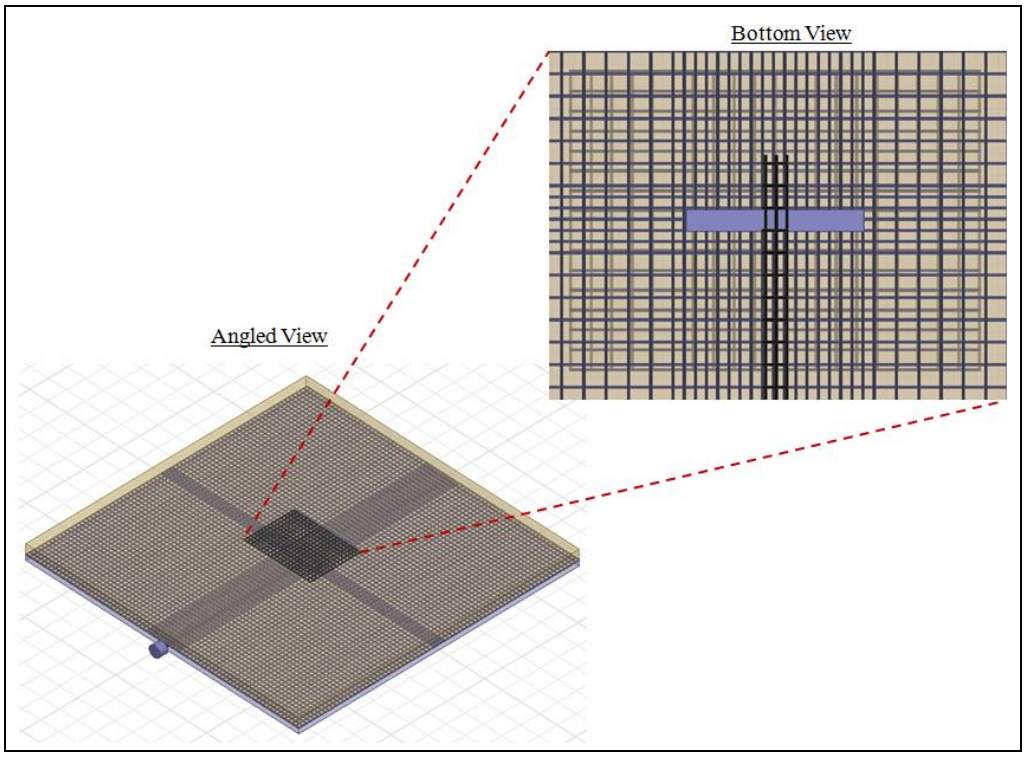

Figure 38. Meshed CNT thread patch antenna with fully meshed feedline and ground plane.

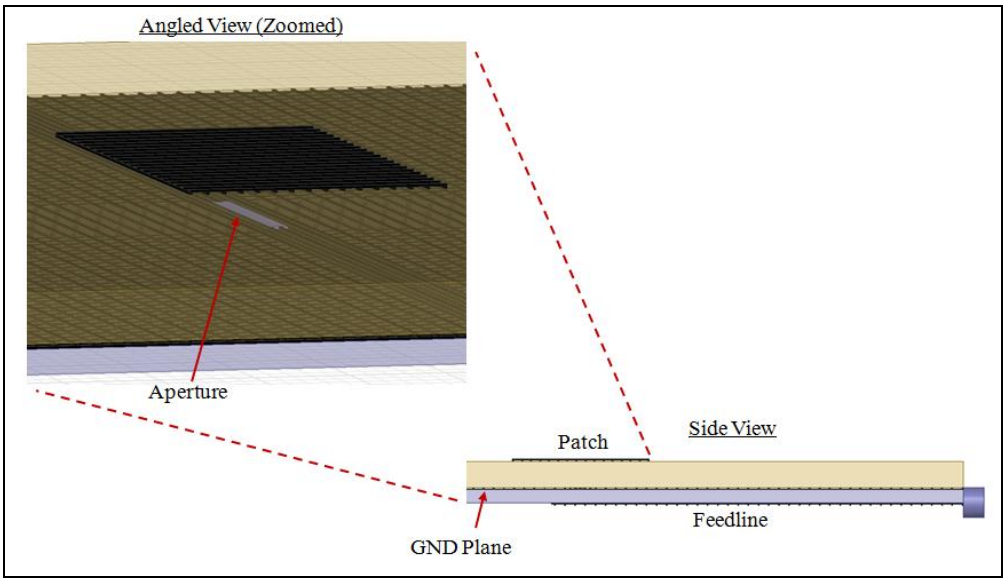

Figure 39. Cross-sectional view of CNT thread patch antenna with fully meshed feedline and ground plane.

The reflection coefficient data shown in figure 40 indicate that the S_{11} will improve as the feedline and GND plane are constructed from CNT meshed thread. The $S_{11} < -10$ dB bandwidth also increases well beyond that of the baseline case, indicating a better and broader input impedance match for these designs. While these characteristics look promising, the E-plane radiation pattern data in figure 41 show the cost of replacing high-conductivity copper material with moderate conductivity meshed CNT thread material for the feedline and GND plane. When the antenna feedline is fabricated from meshed CNT thread, the realized gain of the antenna drops from 5.2 to 0.9 dBi—a reduction to under 40% of the radiated power level for the baseline case. When the GND plane is also fabricated from meshed CNT thread, the realized gain is further reduced to less than –1.8 dBi—a further reduction to under 20% of the baseline case radiated power level. The drop in realized gain is likely due to increased conductor losses in the meshed feedline and GND plane that overshadow the reduction in impedance mismatch losses.

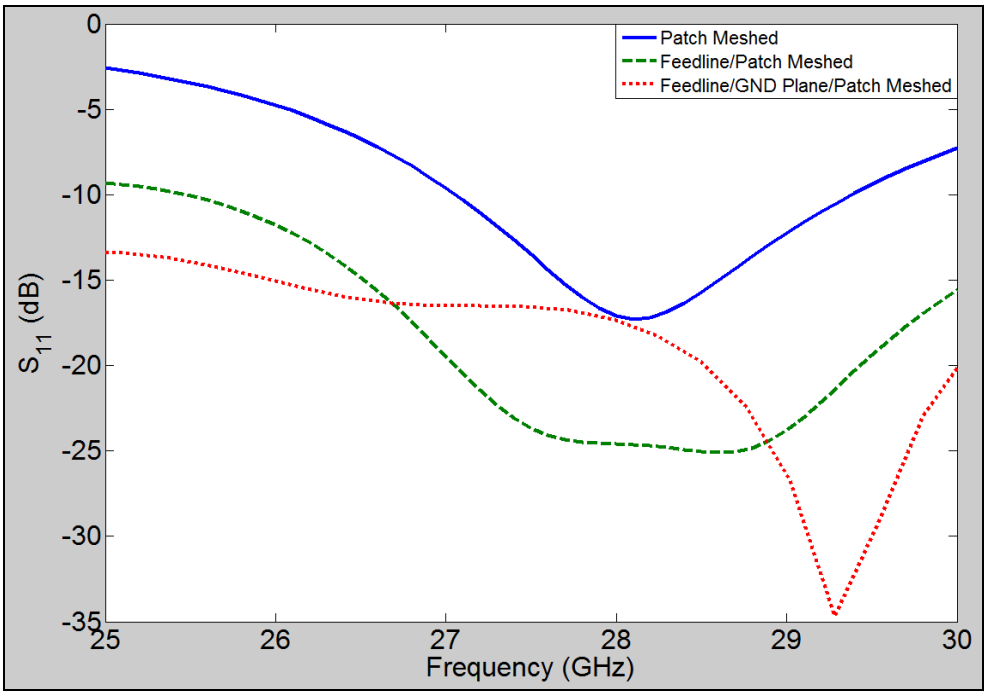

Figure 40. Effect of meshed feedline/GND plane on reflection coefficient for meshed CNT thread patch antennas.

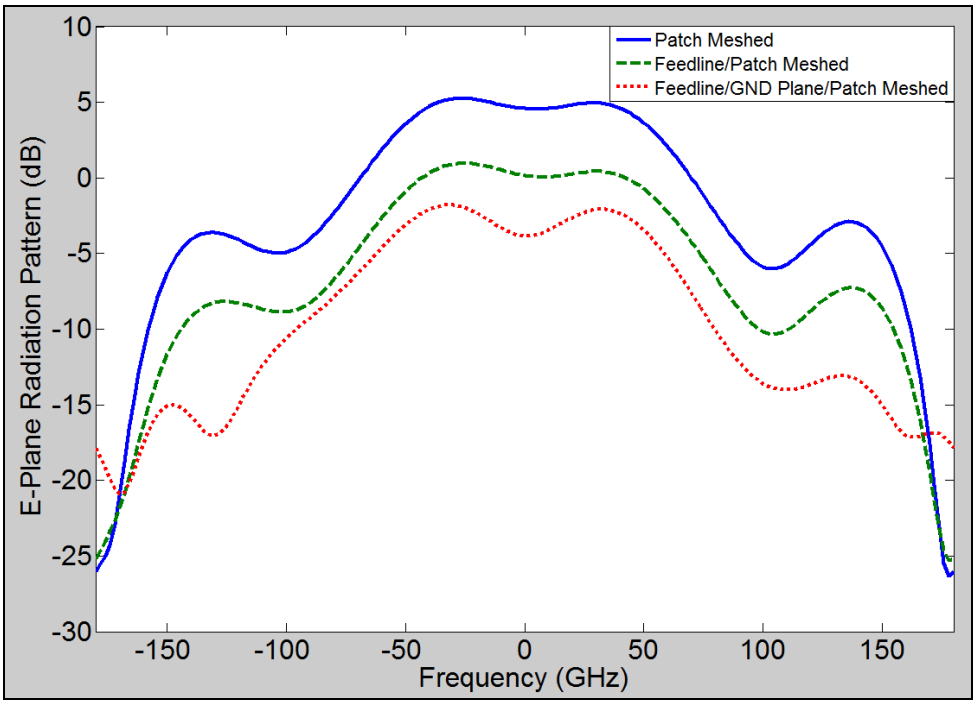

Figure 41. Effect of meshed feedline/GND plane on radiation pattern for meshed CNT thread patch antennas.

Thus, while the impedance match and bandwidth may improve by fabricating the entire antenna from the meshed CNT thread material, the reduction in realized gain will have a severe impact on the radiation performance of the antenna. It is expected that by improving the conductivity of the CNT thread material above its current measured value of 3e4 S/m, the realized gain for these examples may be improved.

4. Conclusions and Future Work

Year 2 of this DRI focused on the fabrication and measurement of a variety of CNT thread and sheet antenna designs, as well as on the development of an innovative multifunctional CNT patch antenna/gas sensor. By comparing these prototypes to a baseline prototype constructed from standard conductive material (e.g., copper), we were able to evaluate the benefits and tradeoffs of employing bulk CNT materials as the radiating elements in Army antenna designs.

A variety of CNT thread/rope dipole and loop antennas were fabricated, measured, and compared with a standard copper dipole antenna. Initial results were inconclusive, potentially due to poor electrical contact between the SMA connector and the CNT thread and/or due to poor balun designs. Subsequent measurements were conducted on just one leg of the dipole in order to examine a λ/4 stub antenna without the influence of a balun. Results were accurate for the copper prototype but were poor for all CNT prototypes, indicating that either electrical contact with the connector was poor and/or that the CNT thread was acting as a very poor radiator. A subsequent prototype CNT thread loop antenna was fabricated with the feedpoint connection and balun issues improved. Measured results from this prototype were successful and agreed reasonably well with loop antenna theory. Since feedpoint issues remained a concern, a reliable comparison with a standard copper prototype was still not possible.

In order to circumvent the existing unreliable feedpoint connection fabrication issues, a variety of aperture coupling feed technique was employed with a patch antenna design. This technique employed an indirect feedline mechanism to the patch antenna, with a reliable copper feedline used to ensure a consistent feedpoint connection and a radiation method in which energy was coupled from this feedline up through an aperture to excite the radiating patch. With this technique, no physical contact was required between the connector and the CNT sheet material. A variety of aperture-coupled patch antenna prototypes were constructed from CNT sheet material and copper tape in order to evaluate the performance of the CNT material as an RF radiator. The thickness of the CNT sheet had a significant impact on the radiation performance of the CNT sheet patch antenna prototypes, with a patch antenna constructed from 5-μm-thick CNT sheet exhibiting a much better reflection coefficient and producing ~5.5 dB higher realized gain than a patch antenna constructed from 0.5-μm CNT sheet. This improvement in RF performance was mainly attributed to lower input reactance. The 5-μm CNT sheet patch antenna exhibited ~2.05-dBi total realized gain compared with ~5.6-dBi realized gain for baseline copper

patch antenna, a ~3.5-dB reduction attributable to the material substitution. It should be noted that the copper was ~17 µm thick, so the reduction in performance for the CNT sheet patch antenna may also be due to its thickness. Research for this design is ongoing and a CNT sheet patch with ~17 µm thickness is currently being fabricated in order to make an explicit performance comparison to the 17-µm-thick copper patch antenna. The performance is expected to improve beyond that of the 5-µm-thick CNT sheet patch antenna. In addition to CNT sheet thickness, an interesting trait of polarization sensitivity was discovered with the CNT sheet material. Optimal RF performance was observed when the CNTs within the CNT sheet material were generally aligned with the E-plane of the patch antenna. When the alignment of these CNTs was rotated to be orthogonal to that of the E-plane of the patch antenna, the RF performance was significantly reduced, resulting in ~8–9 dB lower realized gain and severe input impedance mismatch, mainly from a large increase in input inductance. This will continue to be explored and may have significant applications to polarization-specific antennas and may be useful for improving isolation between neighboring antennas on Army platforms.

Finally, a variation on this design using interwoven CNT threads to form a meshed thread patch antenna was developed and simulated as a concept for a multifunctional communications antenna and reactive gas sensor. Full-wave electromagnetic simulation results indicated the viability of this design to fill both of these roles. By interweaving conducting CNT thread with semiconducting CNT thread, a meshed patch antenna/resonator was designed with a 27.85-GHz resonant frequency and bandwidth of ~2.1 GHz. The predicted effect of an increasing presence of NH_3 around the meshed CNT thread resonator is an approximately linearly downward shift of –60 MHz. This behavior is expected to carry over to other reactive gases, including nitrogen dioxide (NO_2), O_2, nitrogen (N_2), and carbon dioxide (CO_2) and should be explored in future research. With the appropriate additional gas sensor circuitry, this design may be used to simultaneously radiate signals as a satellite communications (SATCOM) antenna and track the presence of a surrounding reactive gas as a resonator gas sensor.

The effects of thread spacing and of fabricating the feedline and ground plane from CNT thread material for the meshed CNT thread patch antenna were explored through simulation. This study indicated that sufficient antenna radiation efficiency and usable bandwidth is attainable with a thread spacing of $d \leq \lambda/30$. However, as the thread spacing is increased, the antenna bandwidth will shrink. A minor center frequency shift and reduction in gain was also observed when the thread spacing was increased and will need to be accounted for in the design process for the meshed thread patch antenna. For the case in which the feedline and/or ground plane was constructed from meshed CNT thread material in addition to the patch, the impedance match and bandwidth improved. However, with this improvement also came a significant reduction in realized gain that resulted in an overall reduced radiation performance for the antenna. The realized gain is expected to improve for these cases as the CNT thread material conductivity is increased beyond its measured value in FY11 of 3e4 S/m.

Over the course of this two-year DRI, the application of CNT materials to Army antenna designs has been explored through simulation and prototype fabrication and measurement. The main conclusion from this study is that CNT materials are a viable conductive material for Army antenna designs and offer significant physical benefits while yielding minor to significant RF performance reduction, depending on the design. The physical benefits that CNT materials offer, such as high tensile strength and low weight, have been confirmed through sample measurements in FY11 and subsequent post-processing improvements and material measurements in FY12. The electrical tradeoffs of employing CNT materials as RF radiators, including frequency shift and realized gain reduction, have been explored with the fabrication and measurement of a variety of CNT thread and sheet antenna designs. The minimization of this reduction in RF performance is dependent upon the state of the art for the CNT material conductivity, which is being continually improved through fabrication technique research, and on the fidelity of the physical connection made between the RF connector/feedline and the CNT material. The lack of efficient and consistently successful fabrication techniques for establishing this connection between the RF source and the CNT material is clearly the highest risk for the employment of these novel materials and must be improved for these materials to have practical application to Army antenna designs. Future work will focus on solving this problem in order to extend the application of this material to Army antenna designs beyond the technical readiness (TR)3/TR4 level. Improvements to the physical and electrical characteristics of the CNT thread and sheet materials will be an ongoing aspect of future work and will lead to increased performance and lower fabrication costs. Future work will also place specific emphasis on textile-integrated CNT thread designs, particularly on the fabrication of CNT thread designs with the use of a sewing machine, in order to produce lightweight, durable clothing/backpack/tent-integrated antennas for Army systems.

This work has lead to significant advances to the existing body of research on RF applications for CNT materials. Specific advancements include the fabrication and measurement of CNT sheet patch antennas; the concept, design and simulations of a meshed CNT thread patch antenna and gas sensor; and the case study on the impact that CNT thread spacing will have on the performance of a meshed thread patch antenna. The research conducted for each of these advancements will be published in peer-reviewed journals in FY13 and will contribute to future research on RF applications of CNT materials.

5. References

1. Burke, P. J.; Li, S.; Yu, Z. Quantitative Theory of Nanowire and Nanotube Antenna Performance. *IEEE Transactions on Nanotechnology* **July 2006**, *5* (4), 314–334.

2. Hanson, G. W. Radiation Efficiency of Nano-radius Dipole Antennas in the Microwave and Far-infrared Regimes. *IEEE Antennas and Propag. Mag.* **June 2008**, *50* (3), 66–77.

3. Salahuddin, S.; Lundstrom, M.; Datta, S. Transport Effects on Signal Propagation in Quantum Wires. *IEEE Trans. Electron Devices* **August 2005**, *52* (8), 1734–1742.

4. Raychowdhury, A.; Roy, K. Modeling of Metallic Carbon-nanotube Interconnects for Circuit Simulations and a Comparison with Cu Interconnects for Scaled Technologies. *IEEE Trans. Comput.-Aided Des.* **January 2006**, *25* (1), 58–65.

5. Plombon, J. J.; O'Brien, K. P.; Gstrein, F.; Dubin, V. M. High-frequency Electrical Properties of Individual and Bundled Carbon Nanotubes. *Appl. Phys. Let.* **2007**, *90*.

6. Huang, Y.; Yin, W.-Y.; Liu, Q. H. Performance Prediction of Carbon Nanotube Bundle Dipole Antennas. *IEEE Trans. Nanotech.* **May 2008**, *7* (3), 331–337.

7. Choi, S.; Sarabandi, K. Performance Assessment of Bundled Carbon Nanotube for Antenna Applications at Terahertz Frequencies and Higher. *IEEE Trans. Antennas Propag.* **March 2011**, *59* (3), 802–809.

8. Mast, D. The Future of Carbon Nanotubes in Wireless Applications. *Antenna Systems/Short-Range Wireless Conference*, September 2009.

9. Keller, S. D.; Shanov, V.; Schulz, M. J.; Mast, D. B. Simulation and Measurement of Carbon Nanotube Thread Dipole Antennas. *2011 USNC-URSI National Radio Science Meeting Proc.*, July 2011.

10. Keller, S. D.; Zaghloul, A. I.; Nichols, B. *Lightweight, Durable Army Antennas using Carbon Nanotube Technology (FY11 director's research initiative year 1 final report)*; ARL-MR-0803; U.S. Army Research Laboratory: Adelphi, MD, February 2012.

11. Pohls, J.-H.; Johnson, M. B.; White, M. A.; Malik, R.; Ruff, B.; Jayasinghe, C.; Schulz, M. J.; Shanov, V. Physical Properties of Carbon Nanotube Sheets Drawn from Nanotube Arrays. *Carbon* **September 2012**, *50* (11), 4175–4183.

12. Keller, S. D.; Weiss, S. J. Microstrip Patch Antenna Array for a Scalable X-band Radar System. *IEEE Antennas and Propagation Society International Symposium Proceedings*, Toronto, Canada, July 2010.

13. Kong, J.; Franklin, N. R.; Zhou, C.; Chapline, M. G.; Peng, S.; Cho, K.; Dai, H. Nanotube Molecular Wires as Chemical Sensors. *Science* **January 2000**, *287*, 622–625.

14. Ong, K. G.; Zeng, K.; Grimes, C. A. A Wireless, Passive Carbon Nanotube-based Gas Sensor. *IEEE Sensors Journal* **April 2002**, *2* (2), 82–88.

15. Chopra, S.; Pham, A.; Gaillard, J.; Parker, A.; Rao, A. M. Carbon-nanotube-based Resonant-circuit Sensor for Ammonia. *Applied Phys. Lett.* **June 2002**, *80* (24), 4632–4634.

16. Chopra, S.; Pham, A.; Gaillard, J.; Rao, A. M. Development of RF Carbon Nanotube Resonant Circuit Sensors for Gas Remote Sensing Applications. *2002 IEEE MTT-S Digest*, pp. 639–642, 2002.

17. Mcgrath, M.; Pham, A. Carbon Nanotube Based Microwave Resonator Gas Sensors. *Int. J. of High Speed Electr. and Sys.* **December 2006**, *16* (4), 913–935.

18. Mcgrath, M.; Pham, A. Microwave Vertically Aligned Carbon Nanotube Array Sensors for Ammonia Detection. *2005 IEEE Sensors Conference Proceedings*, pp. 837–840, 2005.

19. Wang, Y.; Yeow, J.T.W. A Review of Carbon Nanotubes-based Gas Sensors. *Journal of Sensors* **2009**, *2009*, 1–24.

20. Clasen, G.; Langley, R. Meshed Patch Antennas. *IEEE Trans. Antennas Propag.* **June 2004**, *52* (6), 1412–1416.

21. Mallik, N. et al. Study on Carbon Nano-tube Spun Thread as Piezoresistive Sensor Element. *Advanced Materials Research* **2009**, *67*, 155–160.

6. Transitions

The goal of this research is to ultimately transition flexible, lightweight, durable antenna designs constructed from carbon nanotube materials to weight-restricted Army platforms (e.g., unmanned aerial vehicles [UAVs], micro-autonomous vehicles) and textile integrated RF applications.

Year 2 of this DRI research has produced a Cooperative Agreement (W911NF-12-2-0031) with the University of Cincinnati through the Army Research Office in May 2012 and the following:

6.1 Conference Paper/Presentation

1. Keller, S. D.; Zaghloul, A. I. Multifunctional Meshed Carbon Nanotube Thread Patch Antenna. *IEEE Sensors Conference Proceedings*, Limerick, Ireland, October 2011.

6.2 Journal Publications

1. Keller, S. D.; Zaghloul, A. I.; Shanov, V.; Schulz, M. J.; Mast, D. B. Simulation and measurement of carbon nanotube sheet patch antennas, *IEEE Transactions on Antennas and Propagation*,submitted Jan 2013, under review.
2. Keller, S. D.; Zaghloul, A. I.; Shanov, V.; Schulz, M. J.; Mast, D. B. Electromagnetic analysis and simulation of carbon nanotube thread dipole antennas, *IEEE Transactions on Nanotechnology*, submitted Jan 2013, under review.
3. Keller, S. D.; Zaghloul, A. I.; Shanov, V.; Schulz, M. J.; Mast, D. B. Design and simulation of a meshed carbon nanotube thread patch antenna, *IEEE Transactions on Antennas and Propagation*, submitted Jan 2013, under review.

6.3 Book Chapter

1. Keller, S. D.; Zaghloul, A. I.; Shanov, V.; Schulz, M. J.; Mast, D. B. *Carbon Nanotube Yarn and Sheet for Electromagnetics- Antennas, Shielding*; Nanotube Superfiber Materials, Chapter 24, Elsevier, 2013 [submitted Jan. 2013].

6.4 Patent Application Filed

1. Keller, S. D.; Zaghloul, A. I. Method and Apparatus for Providing a Multifunction Sensor using Mesh Nanotube Material, Patent # 13/686,944.

6.5 ARL Program Reviews

1. 2012 ARL Technical Assessment Board (TAB) Review poster.
2. ARL/SEDD Open House poster.

List of Symbols, Abbreviations, and Acronyms

3-D	three-dimensional
ARL	U.S. Army Research Laboratory
CNTs	carbon nanotubes
CO_2	carbon dioxide
CVD	chemical vapor deposition
DMSO	dimethyl sulfoxide
DRI	Director's Research Initiative
ESEM	electron scanning microscope
GND	ground
HFSS	High Frequency Structure Simulator
HPBW	half power beamwidth
MWNT	multiwall nanotubes
N_2	nitrogen
NH_3	ammonia
NO_2	nitrogen dioxide
O_2	oxygen
PEC	perfect electric conducting
RF	radio frequency
SATCOM	satellite communications
Si	silicon
SWNT	single-wall nanotube

No of. Copies	Organization
1 PDF	DEFENSE TECH INFO CTR ATTN DTIC OCA 8725 JOHN J KINGMAN RD STE 0944 FT BELVOIR VA 22060-6218
11 HCS	US ARMY RSRCH LAB
3 CDS	ATTN IMAL HRA MAIL & RECORDS MGMT (1 CD) ATTN RDRL CIO LL TECHL LIB (1 CD) ATTN RDRL SER M A ZAGHLOUL (1 HC) ATTN RDRL SER M E ADLER (1 HC) ATTN RDRL SER M S KELLER (7 HCS, 1 CD) ATTN RDRL SER M S WEISS (1 HC) ATTN RDRL SER P AMIRTHARAJ (1 HC) ADELPHI MD 20783-1197

TOTAL: 15 (1 PDF, 11 HCS, 3 CDS)

INTENTIONALLY LEFT BLANK.